Coordination Chemistry Reviews 253 (2009) 2891–2911

Contents lists available at ScienceDirect

Coordination Chemistry Reviews

journal homepage: www.elsevier.com/locate/ccr

Review

# Molecular engineering for synthesizing novel structures of metal–organic frameworks with multifunctional properties

Shilun Qiu*, Guangshan Zhu

*State Key Laboratory of Inorganic Synthesis & Preparative Chemistry, Jilin University, 2699 Qianjin Street, Changchun 130012, China*

**Contents**



ARTICLE INFO

*Article history:*
Received 21 January 2009
Accepted 27 July 2009
Available online 4 August 2009

*Keywords:*
Metal–organic frameworks
Secondary building unit
Topology
Adsorption
Chiral

ABSTRACT

Metal–organic frameworks (MOFs) which are constructed from metal ions or metal ion clusters and bridging organic linkers, have recently emerged as an important family of porous materials due to their unique structural and functional properties. This review provides the molecular engineering for synthesizing novel MOF structures and summarizes their potential applications. In this review, we present the promotion of the synthesis chemistry in this area and introduce the general methods and the important factor of organic template in the synthesis process. To obtain MOFs with high porosity, three strategies will be introduced. We also discuss how to functionalize the MOFs from two directions: chiral frameworks and frameworks constructed from rare earth metals. The burgeoning area of MOF membranes will also be introduced. Most applications of MOFs are based on their ability to function as hosts. The potential applications including hydrogen storage and methane storage, molecular separation, catalysis, and sensor, are summarized. It is expected that MOFs will provide extraordinary advantages over traditional porous materials and have an important and permanent impact on the future of porous compounds.



*Abbreviations:* adip, 5,5′-(9,10-anthracenediyl)di-isophthalate; asp, aspartic acid; BDC, 1,4-benzenedicarboxylate; bipy, bipyridine; 4-btapa, 1,3,5-benzene tricarboxylic acid tris[*N*-(4-pyridyl)amide; bpdc, 4,4′-biphenyldicarboxylate; BTC, 1,3,5-benzenetricarboxylate; BTB, 1,3,5-benzenetribenzoate; BTT, 1,3,5-benzenetristetrazol-5-yl; CHA, cyclohexylamine; CTC, *cis*,*cis*-1,3,5-cyclohexanetricarboxylate; DDBB, (R)-6,6′-dichloro-2,2′-dihydroxy-1,1′-binaphthyl-4,4′-bipyridine; DEF, diethylformamide; DETA, diethylenetriamine; DMA, *N*,*N*-dimethylacetamide; DMF, *N*,*N*-dimethylformamide; DMSO, dimethyl sulfoxide; $E_3HB$, ethyl-3-hydroxybutyrate; EtOH, ethanol; FOS, functional organic site; hfipbb, 4,4′-(hexafluoroisopropylidene) bis(benzoate); hmmi, 2-hydroxymethyl-1-methylimidazole; hmt, hexamethylenetetramine; im, imidazolate; ImDC, 4,5-imidazoledicarboxylate; IPA, isopropanolamine; JUC, Jilin University China; L-lac, L-lactic acid; MOF, metal–organic framework; NTB, 4,4′,4″-nitrilotrisbenzoate; PCP, porous coordination polymers; PDA, p-phenylenediacrylate; PDC, pyridine-2,5-dicarboxylate; PIP, piperazine; PTMTC, 4,4′,4″-methanetriyltris(2,3,5,6-tetrachlorobenzoate); pyz, pyrazine; pzdc, pyrazine-2,3-dicarboxylate; QS, 8-hydroxyquinoline-5-sulfonate; SBU, secondary building unit; TA, tartaric acid; TBA, tri-*n*-butylamine; tbip, 5-tert-butylisophthalate; TEA, triethylamine; TPA, tri-*n*-propylamine; UMC, unsaturated metal center; UMS, unsaturated metal site; ZIF, zeolitic imidazolate framework.

* Corresponding author. Tel.: +86 431 85168589; fax: +86 431 85168589.
*E-mail addresses:* sqiu@mail.jlu.edu.cn (S. Qiu), zhugs@mail.jlu.edu.cn (G. Zhu).

0010-8545/$ – see front matter © 2009 Elsevier B.V. All rights reserved.
doi:10.1016/j.ccr.2009.07.020

## 1. Introduction

During the past 10 years, metal–organic frameworks (MOFs, also known as porous coordination polymers (PCPs)) have attracted wide scientific attention, as can be seen from the increasing number of publications devoted to this field [1]. Such high interest is caused not only by the enormous variety of interesting molecular topologies but also owing to their excellent properties, with promising applications such as the storage of gases, molecular separation from the gaseous and liquid mixtures, catalysis, sometimes showing the enantioselectivity, and sensors for special classes of molecules [2,3]. They also can be designed as multifunctional materials with excellent physical properties like magnetism, luminescence, and optoelectronics [4–8]. However, the majority of these applications are based on the ability of MOFs to behave as hosts for certain molecules. MOFs have already been tested as microporous materials with exceptionally high porosity, uniform but tunable pore size and with well-defined molecular adsorption sites. Many metal–organic frameworks are now reported in the literatures with surface areas greater than 1000 $m^2 g^{-1}$, while some surface areas reported in MOFs have exceeded 5000 $m^2 g^{-1}$, such as MIL-101, UMCM-1, etc. [9,42]. One of the most important goals in the synthesis of new materials is to achieve real "design" and to obtain compounds with expected structures and properties.

Generally speaking, MOF structures have two main components: the organic linkers and the metal centers. The organic linkers considered as organic secondary building unit (SBU), act as "struts" that bridge metal centers considered as inorganic SBU, which in turn act as "joints" in the resulting MOF architecture [10,11]. The two main components are connected to each other by coordination bonds, together with other intermolecular interactions, to form a network with a definite topology.

Metal centers in MOF structure are usually metal clusters, like metal–carboxylate clusters, metal–azolate clusters, etc. (Fig. 1) [12,13], sometimes just metal atoms or rod-shaped clusters [11]. The coordination number and geometries of metal centers rule the inorganic SBU nodes in the target network. However, the challenge to produce the target network structure from the reactions of simple metal ion and organic linkers is that free metal ions contain too many binding sites and have little directional information. The promotion of inorganic synthesis chemistry to needed to solve this problem. The concept inorganic SBU borrowed from the description of zeolites facilitates the design and synthesis of the extended frameworks. The organic linkers are multidentate organic ligands, which are usually carboxylates, azoles, nitriles, etc. (Fig. 2) [10]. The ligands can also be designed for the nodes in the target network, and can be synthesized and modified by organic synthesis. The properties of the metal centers and linkers usually determine the function of the target material, like porosity, pore size, pore surface and other physical properties [2]. If the nodes of network are well-defined, the network structure could possibly be predicted (Fig. 3) [10,14,15]. However, there are a large number of possible structures for each geometrical shape, which is another big challenge in the molecular engineering of MOF materials. For example, more than 100 different topologies are possible for linking tetrahedral building blocks together into structures with just one kind of vertex (that is, all vertices related by symmetry), like diamond, the zeolite topologies, etc. Research reveals that only a small number of simple, high-symmetry structures will be expected to form most commonly. More complicated structures can be targeted by judicious use of appropriately shaped inorganic SBUs and linkers, and the consideration of effects of the solvent and template and reaction conditions [10,16].

One of the most important objectives is the design of a third generation of molecular sieve, with large, regular, accessible cages and tunnels [17,18]. There are many strategies to achieve large pores and high porosity. In this review, we will introduce three which are mainly considered from three important elements of MOF: topology of framework, inorganic metal centers, and organic ligands:

(1) Synthesizing four-connected and porous MOFs with zeolite topology: by designing inorganic and organic four-connected nodes, the structures of MOFs with expanded zeolite topology would have larger pores and higher porosity than zeolites.
(2) Synthesizing MOFs constructed from large metal clusters. Large metal clusters replace a vertex in a network, expanding the size of inorganic SBUs and the dimensions of the network, which leads to large pore size and high porosity.
(3) Synthesizing MOFs with larger or longer organic linkers. Larger or longer organic ligands would expand the length of linker between inorganic SBU, benefitting large pore diameter and also high porosity just as metal clusters would. Owing to the maturity of organic synthesis, this strategy has proven to be more effective and easier to implement.

Although there are challenges in rational syntheses, MOFs allow systematic engineering of chemical and physical properties and structures through the choice and modifications of their components.

## 2. Synthesis of MOFs with novel structures

### 2.1. Synthetic methods of MOFs

The most traditional and commonly used crystal growth method is solvent evaporation by evaporating or cooling a saturated solution. A wide variety of other methods to obtain metal–organic frameworks have been explored, such as diffusion method, hydro(solvo)thermal method, microwave reaction and ultrasonic methods.

(1) Solvent evaporation method. This technique needs convenient conditions: (a) crystals grow in saturated solutions; (b) solubility increases with temperature and crystals can appear during the cooling step. Using this method, Chen et al. synthesized a dinuclear copper(II)–lanthanide(III) complex bridged by hmmi, $CuLa(mmi)_2(NO_3)_3(H_2O)_2$ [19].
(2) Diffusion method. The principle of this method is to slowly bring into contact the different species: (a) one approach is solvent liquid diffusion. First of all, two layers with different densities are formed; one contains the product in a solvent, another is the precipitant solvent, and these are separated with a solvent layer. The precipitant solvent slowly diffuses into the separate layer and crystal growth occurs at the interface. (b) The other approach is the slow diffusion of reactants by the separation of physical barriers, such as two vials with different sizes. Additionally, gels are also used as diffusion and crystallization media in some cases, especially to slow down diffusion and to avoid precipitation of bulk material. The diffusion method is preferred to obtain single crystals suitable for X-ray diffraction analysis instead of non- or poly-crystalline products, especially if the products are poorly soluble. For example, we mixed $Cd(NO_3)_2{\cdot}4H_2O$ (0.15 g, 0.5 mmol), $H_2$bpdc (0.05 g, 0.25 mmol) and 50.0 mL of DMF in a 100-mL beaker. The mixture was stirred in air for 2 h. Subsequently, TEA (0.5 mL) with DMF (15.0 mL) in a 20-mL vial was sealed into the beaker and slowly diffused in at 60 °C over 3 days. The resulting colorless rod-shaped crystals of JUC-48 were collected in 80% yield based on cadmium [20].
(3) Hydro(solvo)thermal method. This method exploits the self-assembly of products from soluble precursors. It was originally

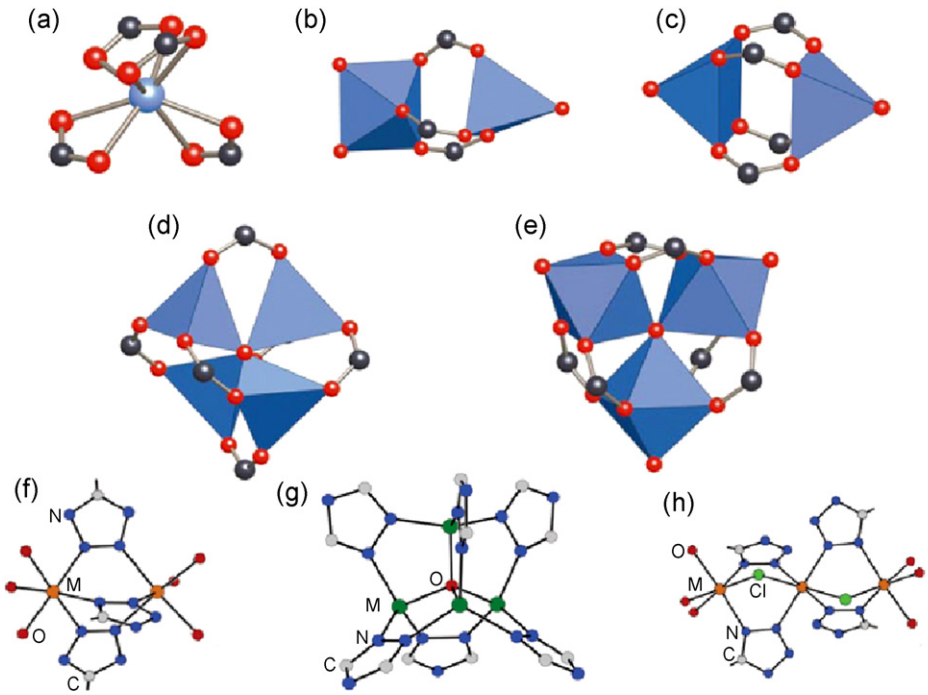


**Fig. 1.** Examples of inorganic SBUs (figure was reproduced from Ref. [10,12], with permission of the copyright holders).

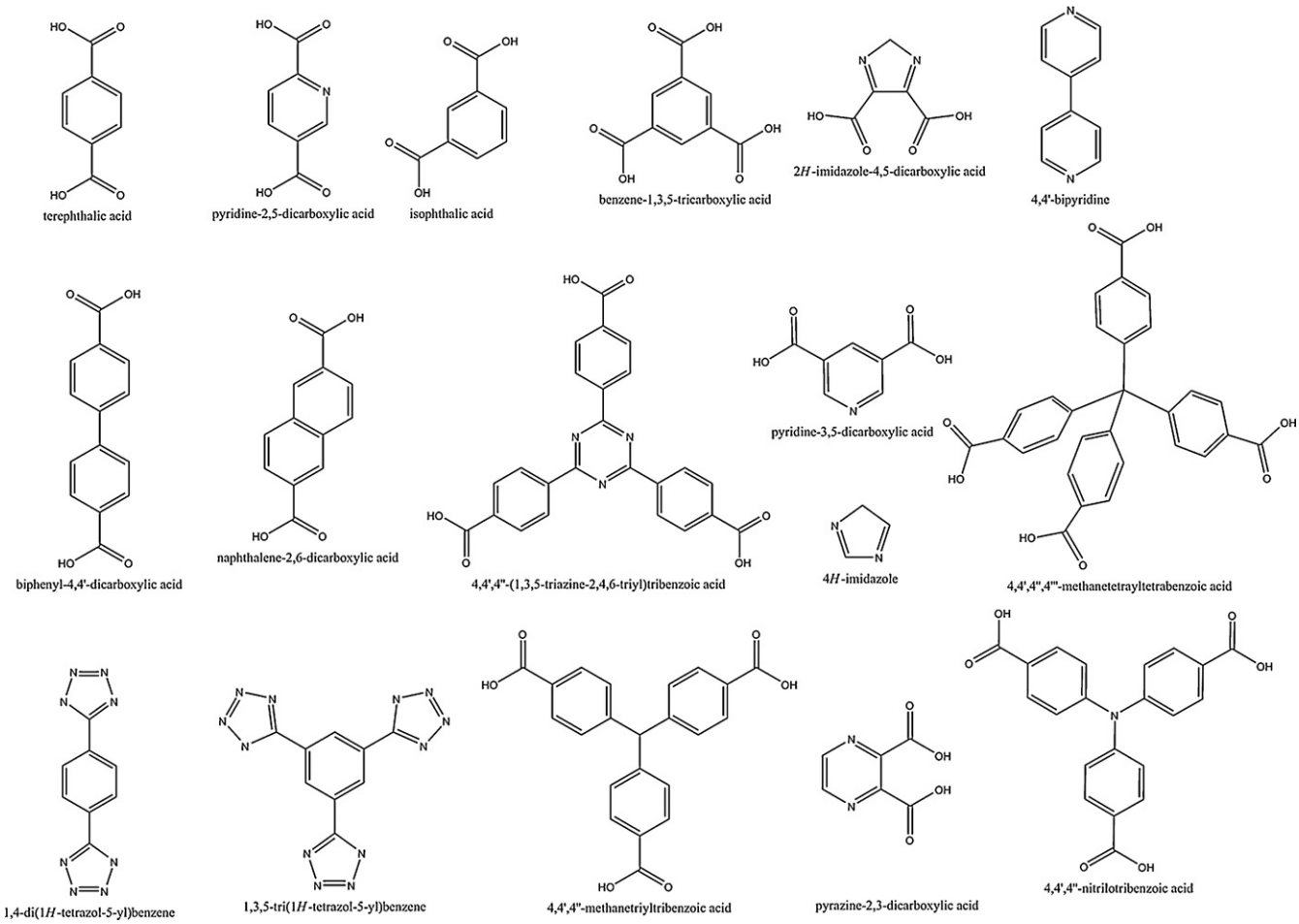


**Fig. 2.** Examples of organic linkers.

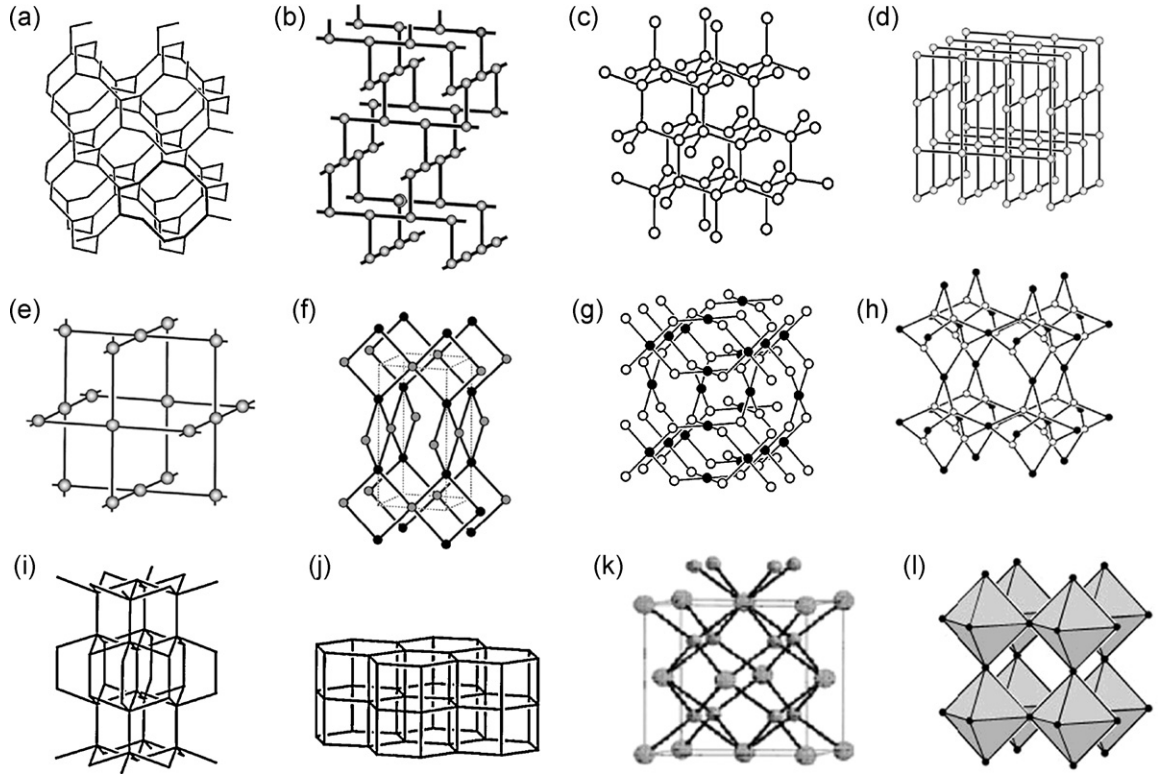


**Fig. 3.** Examples of topologies: (a) $SrSi_2$ net, (b) $ThSi_2$ net, (c) diamond net, (d) $CdSO_4$ net, (e) NbO net, (f) PtS (cooperite) net, (g) $Pt_3O_4$ net (Filled circles are Pt), (h) boracite net, (i) BN net, (j) BCT net, (k) body-centered cubic net, and (l) $ReO_3$ arrangement of corner-sharing octahedral (figure was reproduced from Ref. [14], with permission of the copyright holders).

used for the synthesis of zeolites, but has been adapted to the synthesis of MOFs. The operational temperature range is 80–260 °C inside a closed space (autoclave) under autogenous pressure. This can be influenced mainly by the rate of cooling speed at the end of the reaction. For example, we dissolved $Zn(NO_3)_2{\cdot}6H_2O$ (0.074 g) and (S)-$HO_3PCH_2NHC_4H_7CO_2H$ (0.053 g) in $H_2O$ (10 mL), and then TEA (0.5 mL) was added while stirring to adjust the pH of the mixture. The mixture (pH = 6) was sealed in a Teflon-lined stainless steel autoclave after stirring for 10 min and heated at 160 °C for 2 d. Colorless block single crystals (JUC-14) were filtered off, washed with distilled water, and dried at room temperature (0.079 g, 58%) [21].

(4) Microwave reaction and ultrasonic methods. These are so far, not often used for the preparation of crystalline MOFs, but are an invaluable technique to perform high speed synthesis. It is also a good method to control the size and the shape of the resulting particles. For example, Masel et al. use a conventional microwave to nucleate crystal growth. This MOF synthesis can be completed in 30 s to 2 min. The yield goes from ~30% to over 90%. Additionally, the particle size can be controlled by varying the precursor concentration [22].

### 2.2. Synthesis of MOFs with organic templates

Generally speaking, MOFs are formed by using transition-metal ions as nodes and multidentate organic ligands containing O- or N-donors as linkers. Although many MOFs have been synthesized so far, it is still a challenge to explore successful synthetic strategies for the preparation of the MOFs that have expected applications and intriguing structures. The self-assembly of the frameworks is heavily influenced by factors such as the structural characteristics of the ligands, coordination nature of metal ions, the solvent system, the template, the pH value of the solution, steric requirement of the counterion, reaction temperature and the ratio of metal to ligand etc. In the syntheses of MOFs, the organic molecules (including organic solvent and organic amine) play three different roles in the formation of various types of structures: (1) as a solvent for organic solvent (or an agent to deprotonate O-donor ligands for organic amine); (2) as a structure-directing agent; (3) as a ligand to coordinate to the metal ion [23].

Yaghi and co-workers have successfully synthesized a series of Zn–BTC frameworks by employing different solvents and organic bases [24]. The dimensionality of the resulting Zn–BTC framework is mainly dependent on the solvent media and the strength of organic base.

Recently, Zaworotko et al. reported two very interesting Zn–BTC compounds, $[\{[Zn_6(BTC)_4(isoquinoline)_6(MeOH)]H_2O(benzene)_2\}_n]$ (USF-3), and $[\{[Zn_6(BTC)_4(isoquinoline)_4(MeOH)_2](MeOH)_8(chlorobenzene)\}_n]$ (USF-4), in the presence of different solvents, such as benzene or chlorobenzene [25].

We have reported the synthesis and crystal structures of seven MOFs, $[Cd(HBTC)_2]$ 2(HDETA)·4($H_2O$) (JUC-49), $[Cd_2(BTC)_2(H_2O)_2]$·2(HCHA)·2(EtOH)·2($H_2O$) (JUC-50), $[Cd_5(BTC)_4Cl_4]$·4(HTEA)·2($H_3O$) (JUC-51), $[Cd_3(BTC)_3(H_2O)]$·(HTEA)·2($H_3O$) (JUC-52), [Zn(BTC)($H_2O$)] (HTPA)·($H_2O$) (JUC-53), [Cd(BTC)]·(HTPA)·($H_2O$) (JUC-54), and $[Cd_2(BTC)(HBTC)]$·(HTBA)·($H_2O$) (JUC-55), by using different organic amines as templates. Such amines include DETA, CHA, TEA, TPA, and TBA (Fig. 4) [26].

Remarkably, the organic amine cations reside in the interlayer or channel space, playing important roles such as templating, space-filling, and charge-balancing agents (Fig. 5). For 2D network, the layers of JUC-49 and JUC-53 are held together via hydrogen bonds between the oxygen atoms of carboxylate groups of BTC and the nitrogen atoms of organic amine cations. Because the HTPA molecule is more contorted than the HDETA molecule, the structure of JUC-53 templated by HTPA is an undulated layer, while the framework of JUC-49 templated by HDETA is a planar sheet.

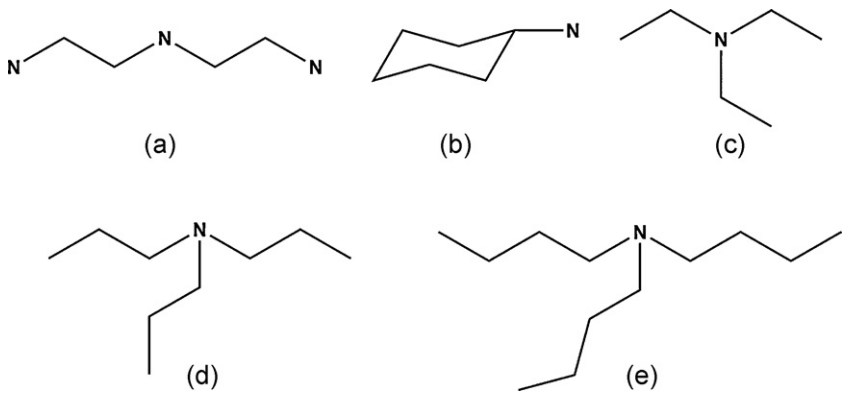


**Fig. 4.** Representation of organic amines: (a) DETA, (b) CHA, (c) TEA, (d) TPA and (e) TBA.

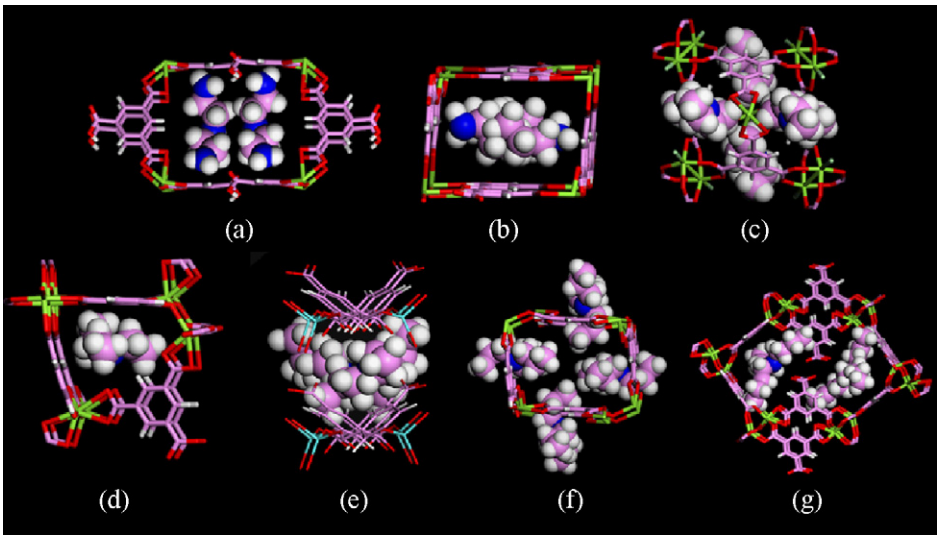


**Fig. 5.** View of different organic amine cations residing in the interlayer or channel space to play roles such as templating, space-filling, and charge-balancing. From (a) to (g), the corresponding compounds are JUC-49 to JUC-55 (figure was reproduced from Ref. [26], with permission of the copyright holders).

However, as for 3D open MOFs, the different organic amine cations are trapped in the vacancies of JUC-50, JUC-51, JUC-52, JUC-54, or JUC-55, which also connect to the framework via hydrogen bonds between the oxygen atoms of BTC and the nitrogen atoms of the organic amine cations, thereby generating their 3D extended networks. In the structures of JUC-50, JUC-52, and JUC-55, the organic amines are located in the center of the channels, and their dimensions (HCHA: 5.4 Å, TEA: 4.9 Å and TBA: 9.7 Å) are similar to those of channels (JUC-50: 7.5 Å, JUC-52: 5.4 Å, JUC-55: 10.1 Å, and van der Waals radii of the atoms have been taken into account), whereas the organic amine molecules in JUC-54 are located between those channels and fill the corresponding space. More interestingly, the HTEA molecules in JUC-51 are located only in cagelike structures, while compound JUC-51 maintains a very open framework (11.5 Å) without guest amines in those channels.

To better understand the templating ability of these organic amines, their non-bonding interaction energies ($E_{inter}$), including H-bonding and van der Waals, have also been studied based on the crystal data by the Cerius$^2$ program [27]. The results are listed in Table 1. The manner of H-bond interactions is important in stabilizing these structures, even though the size and shape of the organic amines are different from one another. Additionally, the values of $E_{inter}$ between the host frameworks and the organic amines are different from each other (from −73.85 to −391.72 kcal mol$^{-1}$ per unit cell), which implies that these organic amines have different structure-directing abilities in the formation of MOF structures.

### 2.3. MOFs with zeolite topologies

MOFs have attracted tremendous attention because of their intriguing molecular topologies. Some structures of minerals, such as diamond, quartz, rutile, perovskite, PtS and feldspar have been artificially produced by replacing monatomic anions ($O^{2-}$, $S^{2-}$) with polyatomic organic ligands as linkers and utilizing the well-defined coordination geometries of metal centers as nodes. However, MOFs with zeolite topologies have rarely been reported because it is difficult to construct 4-connected nodes [30–34].

Férey and co-workers combined targeted chemistry and computational design to create a crystal structure for porous chromium compound, $Cr_3F(H_2O)_2O[(O_2C)C_6H_4(CO_2)]_3{\cdot}nH_2O$ (where $n$ is ∼25, MIL-101), with the augmented zeolite MTN topology by using BDC

**Table 1**
Optimized interaction energies of host–guest ($E_{inter}$) including VDW and H-bond per unit cell of JUC-49 to JUC-55 based on the experimental structural data.

| Polymer | Organic amine | VDW/kcal mol$^{-1}$ | H-bond/kcal mol$^{-1}$ | $E_{inter}$/kcal mol$^{-1}$ |
|---|---|---|---|---|
| JUC-49 | DETA | −239.18 | −152.54 | −391.72 |
| JUC-50 | CHA | −102.28 | −20.27 | −122.55 |
| JUC-51 | TEA | −91.69 | −20.27 | −111.96 |
| JUC-52 | TEA | −61.68 | −12.17 | −73.85 |
| JUC-53 | TPA | −100.57 | −8.97 | −109.54 |
| JUC-54 | TPA | −97.24 | −11.13 | −108.37 |
| JUC-55 | TBA | −132.82 | −19.97 | −152.79 |

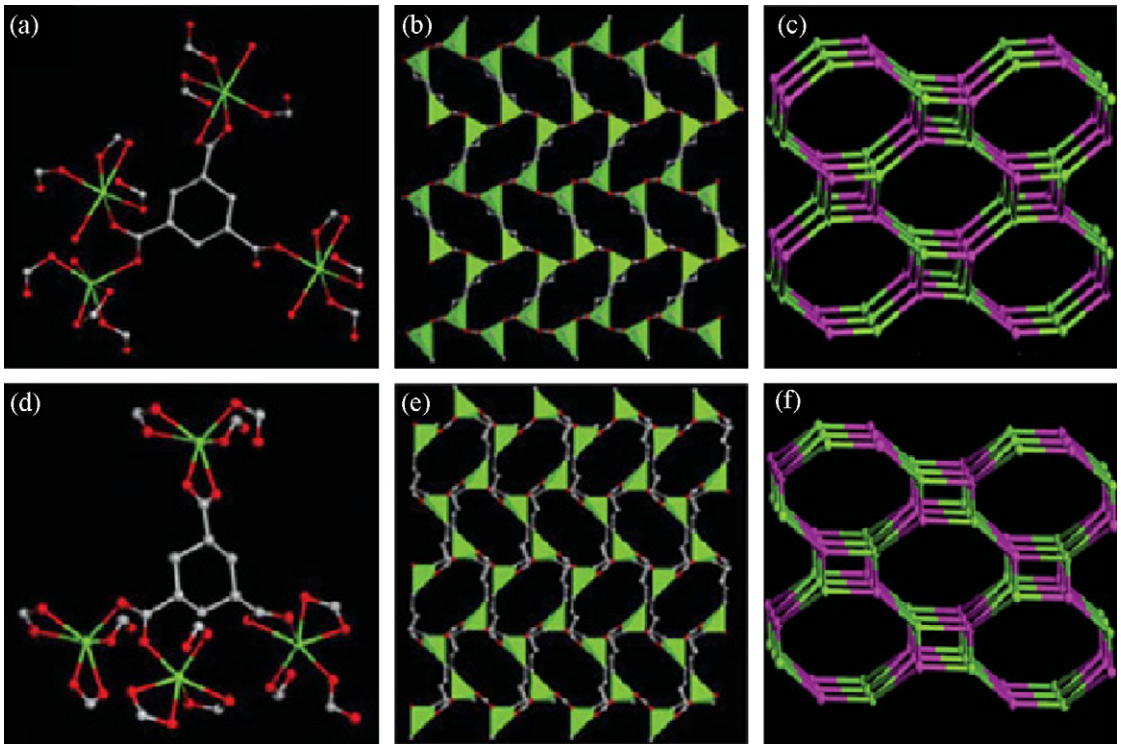


**Fig. 6.** (a) The coordination environments of CTC ligands and cadmium ions in JUC-40. (b) Infinite 3D coordination framework of JUC-40 with about 5 Å × 10 Å elliptical channels viewed along the [1 0 0] direction. (c) The 4-connected nets of JUC-40 with zeolite ABW topology. (d) The coordination environments of cadmium ions and CTC ligands in JUC-41. (e) The 3D network of JUC-41 with about 5 Å × 10 Å elliptical channels viewed along the [1 0 0] direction. (f) The 4-connected nets of JUC-41 with zeolite BCT topology (figure was reproduced from Ref. [39], with permission of the copyright holders).

and $Cr(NO_3)_3$ [7]. Its zeotype cubic structure has the best characteristics in terms of cell dimensions (702,000 $Å^3$), pore sizes (29–34 Å), and surface area (5900 $m^2\,g^{-1}$). Beside the usual properties of porous compounds, this solid has potential as a nanomold for monodisperse nanomaterials by the incorporation of Keggin polyanions within the cages.

We reported two novel 3D MOFs, $Cd(CTC)(H_2O)\cdot(H_2PIP)_{0.5}(H_2O)$ (JUC-40) with zeolite ABW topology (zeolite ABW represents the aluminosilicate zeolite discovered by Barrer and White) [28] and Cd(CTC)·(HIPA) (JUC-41) with zeolite BCT topology (zeolite BCT represents the body-centered tetragonal tectosilicate reported by Dollase and Ross) (Fig. 6) [29,39]. They were synthesized by constructing inorganic and organic 4-connected building units and using the organic bases as templates (PIP or IPA). These frameworks of JUC-40 and JUC-41 not only expand the original structures of zeolites ABW and BCT, but also exhibit significant advantages over them in terms of thermal stability, ion exchange and adsorption.

We have also synthesized a novel 3D MOF, $[\{Cd(H_2O)_3\}_{34}(hmt)_{17}]Cl_{68}\cdot 46(H_2O)\cdot 68(DMF)$ (JUC-27), by building up the metal–organic tetrahedral building block $TM_4$ (T = tetrahedrally coordinated molecule; M = transition-metal ion), in which the M–T–M angles range from 108 to 120°. This was constructed from an hmt molecule and four cadmium ions (Fig. 7). The novel open-framework metal–organic polymer possesses the zeolite MTN topology with two types of $5^{12}$ and $6^4 5^{12}$ cages. The $6^4 5^{12}$ cage has a volume of about 2522 $Å^3$ (a van der Waals sphere with a diameter of 16.8 Å would just fit inside the void). So the $6^4 5^{12}$ cage of zeolite MTN was largely expanded from ~7 Å and its positive charged framework can be utilized for anion exchange (Fig. 8) [40].

Unlike most zeolites, JUC-27 has a positively charged framework. The charge-balancing chlorine anions in the cages could not be directly located in the crystal structure analysis. However, inductively coupled plasma analysis and mass spectrometric analysis indicated that the molar ratio of cadmium to chlorine is 1:2. Anion exchange was carried out for the cationic framework by substituting $SCN^-$ for $Cl^-$ in the cages. The IR spectra of the exchanged product show new $SCN^-$ bands (2075 $cm^{-1}$); the other signals of the IR spectrum and the powder XRD pattern remain virtually unchanged, which suggests that the skeleton is retained after anion exchange.

In 2006, Eddaoudi and co-workers used ImDC as the bridging linker and indium, a group 13 element, as the metal ion source, to synthesis two novel porous anionic zeolite-like metal–organic frameworks (ZMOFs), rho-ZMOF and sod-ZMOF with extra-large cavities (Fig. 9) [30].

Recently, the invention of zeolitic imidazolate frameworks (ZIFs) has provided materials based on simple zeolite structures [35–38]. The frameworks of these compounds can be formulated as $T(Im)_2$ (Im = imidazolate and its derivatives, T = tetrahedrally bonded metal ion) and are similar to the $SiO_2$ frameworks of (alumino)silicate zeolites; in particular the T–Im–T angle of 145° is close to the Si–O–Si angle typically found in zeolites (Scheme 1). In 2008, Yaghi and coworkers reported the synthesis and characterization of two porous zeolitic imidazolate frameworks, ZIF-95 and ZIF-100, with structures of a scale and complexity previously unknown in zeolites (Fig. 10) [35].

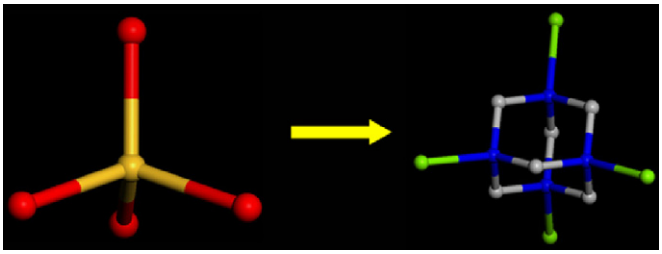

**Fig. 7.** Representation of metal–organic tetrahedral building block $TM_4$ constructed from an hmt molecule and four cadmium ions. (Color code: Cd, green; Si, yellow; O, red; C, grey; N, blue).

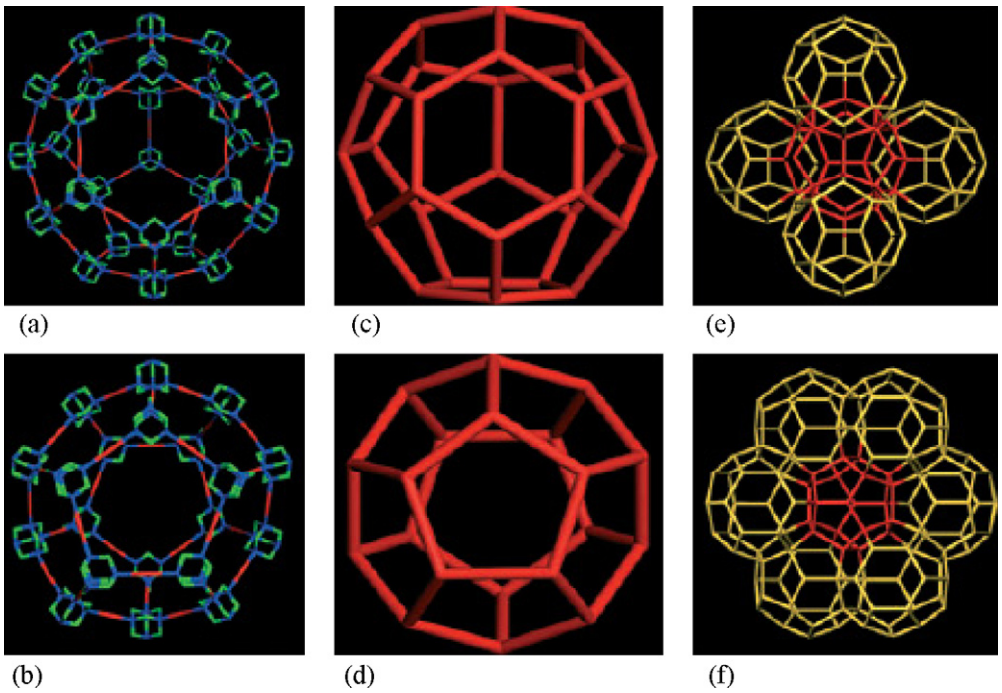


**Fig. 8.** The structure of JUC-27. (a) A large cage constructed from four six-membered rings (six $\{Cd_4(hmt)\}$ tetrahedra) and twelve five-membered rings (five $\{Cd_4(hmt)\}$ tetrahedra). (b) A small cage constructed from twelve five-membered rings (five $\{Cd_4(hmt)\}$ tetrahedra). The topologies of the $6^45^{12}$ and $5^{12}$ cages are shown in (c) and (d), respectively. (e) The $6^45^{12}$ cage in (c; red) sharing its four six-membered rings with four others (yellow). (f) The $5^{12}$ cage in (d; red) sharing its six six-membered rings with six $6^45^{12}$ cages (c; yellow) (figure was reproduced from Ref. [40], with permission of the copyright holders).

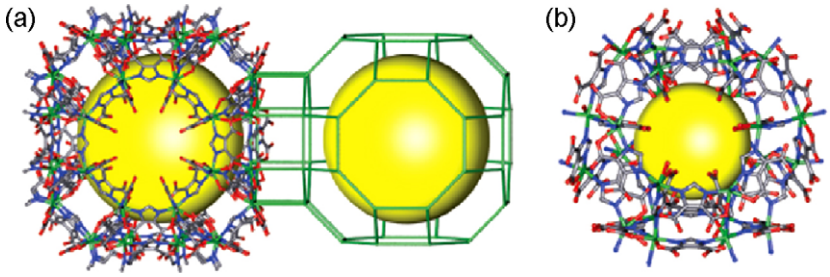


**Fig. 9.** (a) A fragment of the rho-ZMOF, where the yellow spheres represent the largest sphere that would fit in the a-cavities without touching the van der Waals atoms of the framework. (b) A fragment of the sod-ZMOF, the β-cage (figure was reproduced from Ref. [30], with permission of the copyright holders).

### *2.4. MOFs constructed from metal clusters*

The construction of metal carboxylate cluster SBUs is an effective and powerful synthetic method to produce a new generation of highly porous MOFs. Although many MOFs built from different transition-metal carboxylate cluster SBUs have been synthesized, they usually consist of di-, tri-, or tetra-nuclear metal carboxylate clusters, in which water molecule plays an important role as a bridging ligand. It is still a challenge to obtain MOFs with multinuclear metal carboxylate cluster SBUs. However, if the dimensions of these metal carboxylate clusters are expanded further to nanosized SBUs (>10 Å), such MOFs will exhibit characteristics similar to those of nanosized metal oxide semiconducting materials, such as the optoelectronic property.

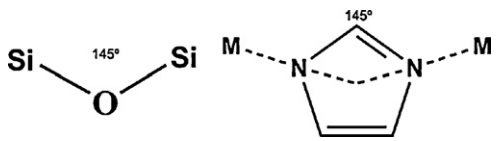


**Scheme 1.** The bridging angles in metal zeolites (left) and IMs (right).

In 1999, Yaghi and co-workers reported the synthesis of a MOF, $Zn_4O(BDC)_3{\cdot}(DMF)_8(C_6H_5Cl)$ (MOF-5), which remains crystalline, as indicated by X-ray single-crystal analyses, and stable when fully desolvated and when heated up to 300 °C. In this structure, an organic dicarboxylate linker (BDC) is used in a reaction that gives supertetrahedron clusters when capped with monocarboxylates.

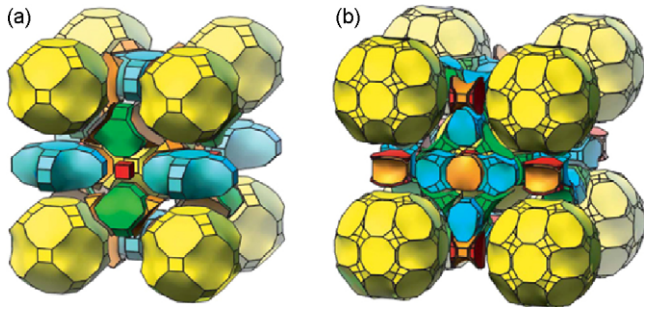


**Fig. 10.** The frameworks of ZIF-95 and ZIF-100 shown as natural tilings. (a) Natural tiling of ZIF-95; the A and B cages are shown in blue and yellow, respectively. (b) Natural tiling of ZIF-100; the giant cage is in yellow (figure was reproduced from Ref. [35], with permission of the copyright holders).

The rigid and divergent character of the added linker allows the articulation of the clusters into a three-dimensional framework resulting in a structure with higher apparent surface area (Langmuir: 2900 $m^2 g^{-1}$) and pore volume (0.61–0.54 $cm^3 cm^{-3}$) than most porous crystalline zeolites [41].

We reported a new 3D MOF, $[Zn_5(\mu_3\text{-}O)_2(bpdc)_4(DMF)_2(EtOH)_2]\cdot 3(DMF)\cdot 3(EtOH)\cdot 5(H_2O)$ (JUC-36), which was synthesized under mild conditions [42]. As shown in Fig. 11, the compound consists of a 3D framework with an expanded diamondoid topology constructed from double 4-connected pentanuclear SBUs, $[Zn_5(\mu_3\text{-}O)_2(OCO)_8]$ with 6.9 Å × 6.9 Å × 9.2 Å, linked by rigid bpdc ligands. For an unusual pentanuclear framework, the compound shows the favorable $CH_3OH$ adsorption behavior (150 mg/g) and good optoelectronic effect (that is, transient photovoltage (PV) signals can be observed when this compound was excited by laser pulses with different intensities), which will facilitate the exploration of new types of multifunctional materials.

We also prepared a novel, three-dimensional, non-interpenetrating microporous metal–organic framework (MOF), $[Zn_7O_2(pda)_5(H_2O)_2]\cdot 5DMF\cdot 4EtOH\cdot 6H_2O$ (JUC-37), synthesized by constructing heptanuclear zinc carboxylate SBUs and by using rigid and linear aromatic carboxylate ligands, PDA [43]. As shown in Fig. 12, the seven zinc centers are held together with ten carboxylate groups of the PDA ligands and four water molecules to form a heptametallic SBU, $Zn_7O_4(CO_2)_{10}$, with dimensions of 9.8 Å × 9.8 Å × 13.8 Å. Furthermore, the heptametallic SBUs are interconnected by PDA acting as linkers, thereby generating an extended network with a three-dimensional, non-interpenetrating, intersecting large-channel system with spacing of about 17.3 Å. As a microporous framework, JUC-37 shows adsorption behavior that is favorable towards $H_2O$ and $CH_3OH$, and substantial $H_2$ uptake. In terms of the heptanuclear zinc carboxylate SBUs, JUC-37 exhibits interesting photoelectronic properties.

Subsequently, we have successfully synthesized the large pore, open-framework complex $[Cd_{11}(\mu_4\text{-}HCOO^-)_6(bpdc)_9]\cdot 9DMF\cdot 6H_2O$ (JUC-35), which contains the largest known undecanuclear $Cd^{II}$–carboxylate cluster SBU, by rationally utilizing a flexible organic acid (HCOOH) as a strong bridging ligand [44] (Fig. 13).

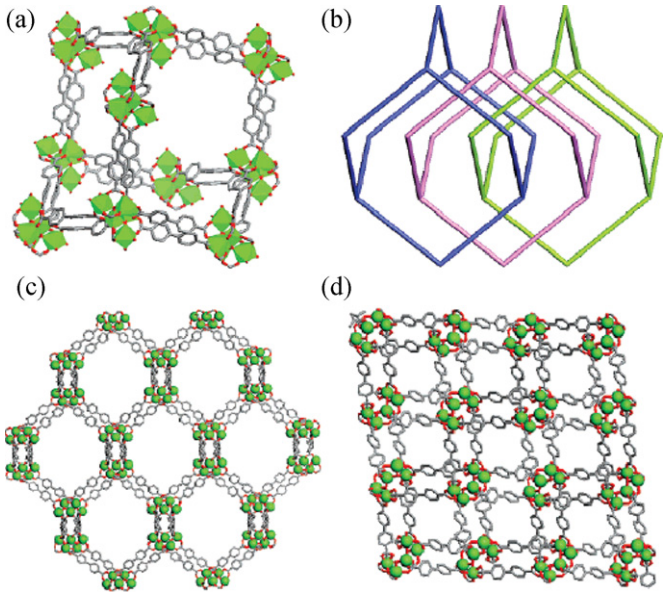


**Fig. 11.** The structure of JUC-36. (a) View of the expanded diamondoid net with the large cavity of approximately 19.4 Å × 31.2 Å. (b) 3D network with the hexagonal channels of 19.7 Å × 24.5 Å expanded from (a). (c) Schematic presentation of the threefold interpenetration. (d) 3D framework viewed along the [1 0 0] direction (figure was reproduced from Ref. [42], with permission of the copyright holders).

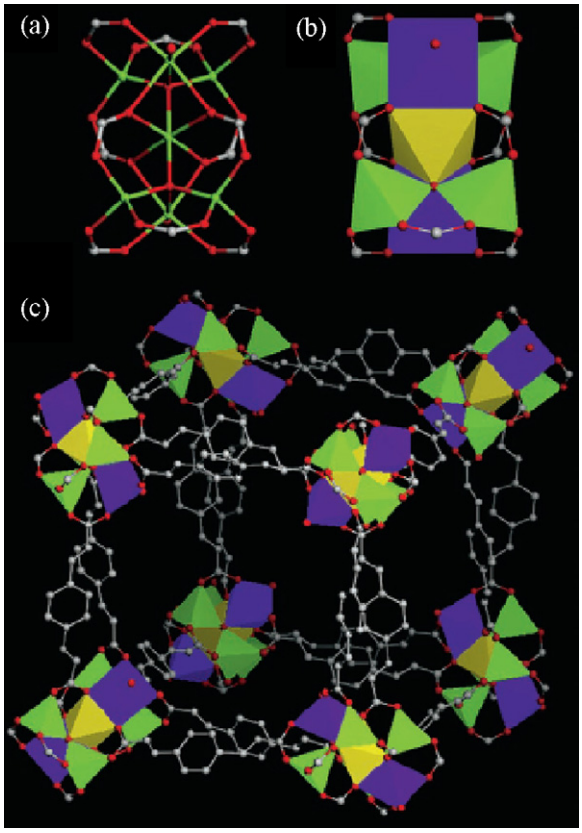


**Fig. 12.** The framework of JUC-37. (a) A ball-and-stick model of the $Zn_7O_4(CO_2)_{10}$ SBU with dimensions of about 9.8 Å × 9.8 Å × 13.8 Å. (b) The same as (a), but with the $ZnO_4$ tetrahedra indicated in green polyhedra and the $ZnO_6$ octahedra indicated in blue or yellow polyhedra for clarity. (c) A view of the cubic cavity constructed from eight SBUs interconnected by PDA acting as linkers (figure was reproduced from Ref. [43], with permission of the copyright holders).

In this structure, each undecanuclear SBU is connected to adjacent SBUs through three biphenyl groups of bpdc molecules along the [001] direction and through two biphenyl groups along three other directions. Therefore, each SBU can be defined as an eight-connected node. On the basis of this simplification, the structure can be described as an eight-connected 3D network with a body-centered cubic (bcu) topology. Additionally, this compound shows good sorption and optoelectronic properties.

At saturation, the amounts of $H_2O$, $CH_3OH$, and $C_2H_5OH$ adsorbed by JUC-35 are 314, 277, and 269 mg $g^{-1}$, respectively, equivalent to the adsorption of approximately 468 molecules of $H_2O$, 234 molecules of $CH_3OH$, and 162 molecules of $C_2H_5OH$ per unit cell. Excited by different intensities of the exciting laser pulse (355 nm), JUC-35 definitely shows the PV transients.

### 2.5. Mesoporous MOFs

Porous MOFs have attracted considerable research interest as they possess a high surface area, modifiable surface and tunable pore size. However, almost all reported open MOFs are microporous (with pore sizes <2 nm), and only limited compounds with channel sizes up to mesoporous range (2–50 nm) were prepared to date [7,45–47]. Ligand extension is an apparent option, but open MOFs built from large ligands tend to collapse upon guest removal and be accompanied by framework interpenetration, which can drastically reduce the size of the pores, thus limiting the entrance of large molecules to the MOF. The construction of mesoporous MOFs must be devised to extend the ligand while inhibiting interpenetration

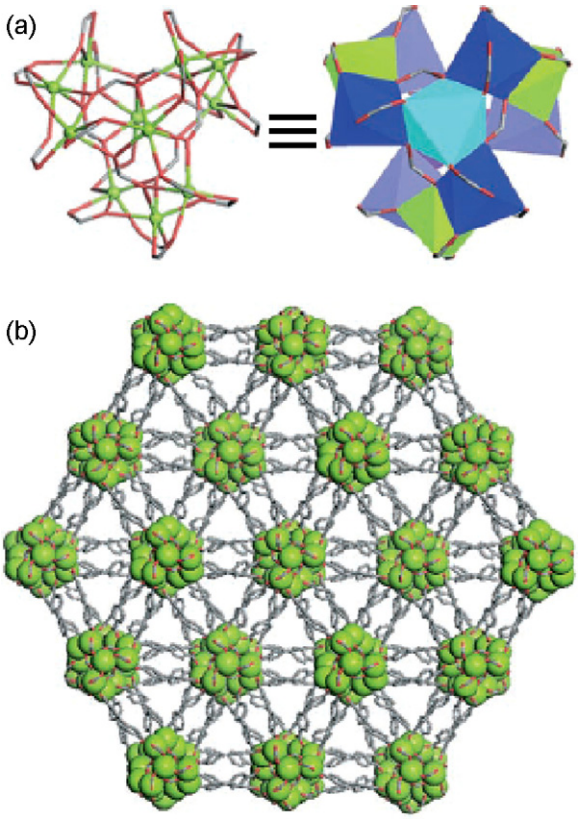


**Fig. 13.** The framework of JUC-35. (a) Ball-and-stick (left) and polyhedral (right) representations of the $Cd_{11}(\mu 4\text{-}HCOO^-)_6(CO_2)_{18}$ SBU. (b) View of the 3D framework along the [0 0 1] direction (figure was reproduced from Ref. [44], with permission of the copyright holders).

and reinforcing the framework against disintegration upon guest removal [48].

In 2006, we successfully synthesized a 3D MOF, $Cd_2(bpdc)_3{\cdot}4(DMF)$ (JUC-60) with a channel constructed of eight homochiral chains with 18.3 Å × 22.4 Å [49] (Fig. 14). To our knowledge, JUC-60 which has the most number of homochiral helical chains has been synthesized for the first time.

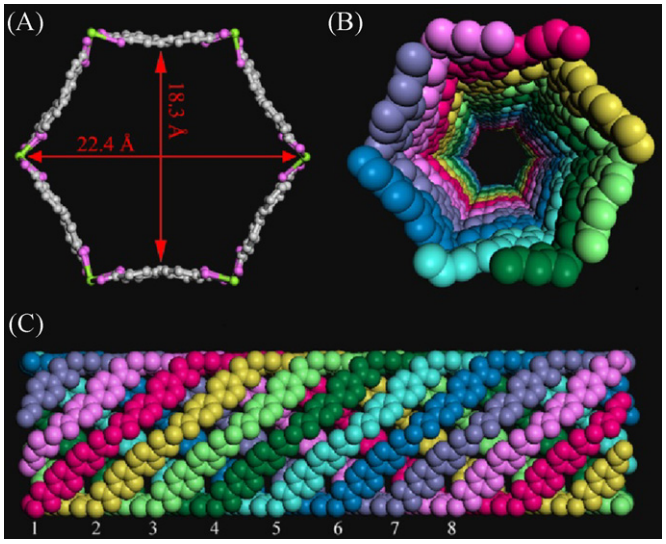


**Fig. 14.** The channel is constructed of eight homochiral helical chains with 18.3 Å × 22.4 Å of JUC-60 (figure was reproduced from Ref. [49], with permission of the copyright holders).

Recently, we successfully synthesized a new MOF, $[Cd_3(bpdc)_3(DMF)]{\cdot}5DMF{\cdot}18H_2O$ (JUC-48), with the largest reported 1D hexagonal nanotube-like channels of 24.5 Å × 27.9 Å and rare etb topology, constructed from rod-shaped cadmium carboxylate SBUs [20] (Fig. 15). This compound exhibits good fluorescence properties and substantial hydrogen uptake (2.8% at 40 bar and 77 K).

### 2.6. MOFs with chiral structures

Chiral MOFs with open frameworks have attracted much attention because of their potential applications in enantioselective separation and catalysis [50–53]. Several approaches have been previously reported for creating chiral materials, including the introduction of chiral ligands or chiral templates, the influence of the chiral physical environment, and spontaneous resolution without any chiral auxiliary [55]. Spontaneous resolution on crystallization without any chiral auxiliary will result in a racemic mixture of enantiomeric crystals [56]. Moreover, spontaneous resolution is relatively rare and cannot be predicted because its mechanism is not yet fully understood. Enantioselective synthesis, however, is a direct and effective method for the synthesis of enantiopure chiral open frameworks by using enantiopure organic building units as reactant precursors. Many chiral open frameworks with high thermal stability have been obtained by enantioselective synthesis in recent years, and they showed encouraging results in enantioselective separation and catalysis.

For example, Kim and co-workers report the synthesis of a homochiral metal–organic porous material, $[Zn_3(\mu_3\text{-}O)(D\text{-}TA)_6]{\cdot}2H_3O{\cdot}12H_2O$ (referred to as D-POST-1), which uses enantiopure metal–organic clusters as SBUs [54].

Lin et al. prepared two homochiral porous MOFs, $[Cd_3(DDBB)_4(NO_3)_6]{\cdot}7MeOH{\cdot}5H_2O$ and $[Cd(DDBB)_2(H_2O)_2]$–$[ClO_4]2{\cdot}DMF{\cdot}4MeOH{\cdot}3H_2O$, built from the same chiral bridging ligand and metal connecting point [55].

In 2004, we chose an enantiomerically pure derivative of (S)-proline, namely, 1-phosphonomethylproline, as a chiral building unit and successfully prepared a homochiral 3D zinc phosphonate $Zn_2[(S)\text{-}O_3PCH_2NHC_4H_7CO_2]_2$ (JUC-14) with alternately arranged left- and right-handed helical channels [21]. As shown in Fig. 16, the 3D framework is based on two crystallographically distinct $ZnO_4$ tetrahedra and two distinct $O_3PC$ tetrahedra. The structure contains four- and eight-membered rings (7 Å × 8 Å), which are made of two different helical chains A and B. These chains run along the b axis and are arranged AA and BB along the *a*-axis, respectively. Of particular interest is that the active sites of 1-phosphonomethylproline for asymmetric catalysis—the amino group and the partially uncoordinated carboxylate group—are retained and directed into the channels, in contrast to a recently reported similar metal phosphonate.

Recently, we synthesized a 2D layer coordination polymer $Co(PDC)(H_2O)2{\cdot}H_2O$ (JUC-25) containing two helical chains by employing an achiral ligand, PDC [56] (Fig. 17). The synthesis did not involve any chiral reactant or solvent or other auxiliary agent. However, the resultant crystals were not racemic as indicated by the observation of strong signals in the vibrational circular dichroism (VCD) spectrum. There is a good agreement between VCD and IR absorption spectra. The vibrational modes were identified and conformational information also can be observed in the VCD spectra. The strong VCD signals indicate that the crystals of $Co(PDC)(H_2O)_2{\cdot}H_2O$ were chiral.

### 2.7. MOFs with rare earth metal centers

Rare earth metals, as functional metal centers, are attracting more and more attention because of their fantastic coordination properties and special chemical characteristics. Rare earth ions have

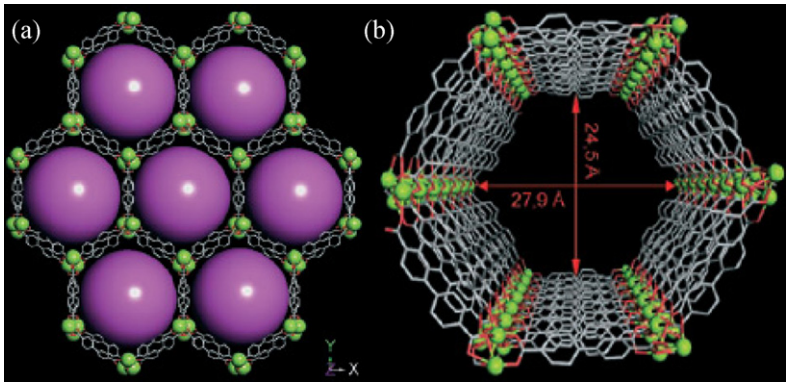


**Fig. 15.** (a) The 3D framework of JUC-48 with 1D hexagonal nanotube-like channels which are indicated by pink spheres of diameter 21.1 Å viewed along the [0 0 1] direction. (b) Representation of a hexagonal nanotube-like channel of dimensions 24.5 Å × 27.9 Å (figure was reproduced from Ref. [20], with permission of the copyright holders).

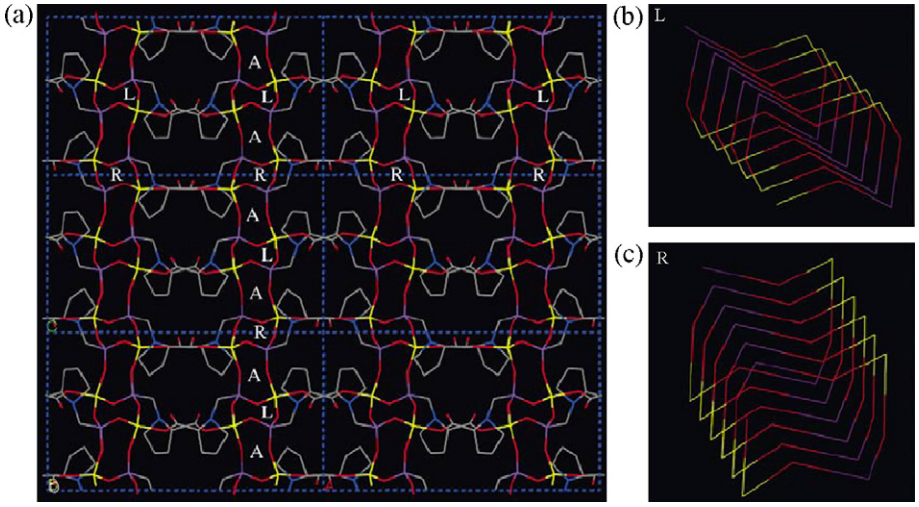


**Fig. 16.** (a) The framework of JUC-14 viewed along the [0 1 0] direction, showing two types of helical channels and achiral channels which are alternately arranged along the c axis (A: achiral channel, L: left-handed helical channel, R: right-handed helical channel). (b and c) The left-handed (L) and right-handed (R) helical channels (figure was reproduced from Ref. [21], with permission of the copyright holders).

high affinity for hard donor atoms and ligands containing oxygen or hybrid oxygen–nitrogen atoms, especially multicarboxylate ligands, which are employed in the architectures of lanthanide coordination polymers. As the high coordination number and flexible coordination geometry of rare earth ions make it difficult to control the preparation of rare earth complexes, the analogous complexes based on rare earth ions are still uncommon compared with those of transition metals [57]. Recently some coordination polymers based on rare earths were synthesized, and most exhibit amazing optical and magnetic properties, enabling them as fluorescent probes and IR-emitters [58–61].

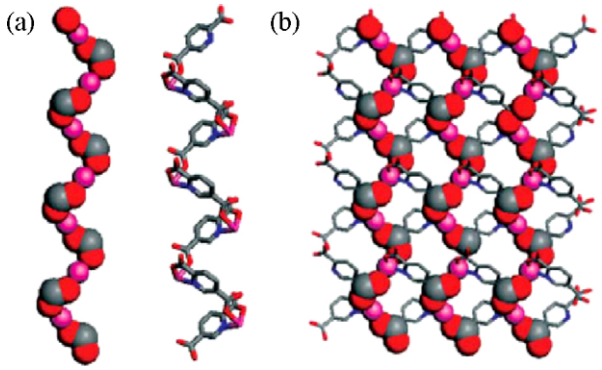


**Fig. 17.** The structure of JUC-25. (a) A space-filling view of the right-handed helical chain of –C–O–Co– and a cylindrical view of the left-handed helical chain of –PDC–Co– along the b axis. (b) The 2D structure including two types of helical chains (figure was reproduced from Ref. [56], with permission of the copyright holders).

For MOFs with rare earth metal centers, we have reported a series of 3D novel compounds $M(bpdc)_{1.5}(H_2O)\cdot 0.5DMF$ (M = Tb, Ho, Er or Y, JUC-28(a–d)) by reaction of the rare earth ions ($M^{3+}$) with bpdc in a mixed solution of DMF and $C_2H_5OH$ [62]. As shown in Fig. 18, they possess the same 3D architectures and crystallize in monoclinic space group C2/c. Two seven-coordinated metal centers and four di-monodentate bpdc groups construct a paddle-wheel building block. These building blocks connect with two carboxyl groups leading to a one-dimensional inorganic chain, —M–O–C–O–M—, along the [0 0 1] direction. The inorganic chains are linked with two biphenyl groups to form 25.15 Å × 17.09 Å rhombic channels along the c axis without interpenetration. These complexes exhibit strong fluorescence in the visible region, and $Er(bpdc)_{1.5}(H_2O)\cdot 0.5DMF$ shows $Er^{3+}$ characteristic emission in the range of 1450–1650 nm at room temperature.

By changing the organic ligand, we prepared a series of microporous lanthanide metal–organic frameworks, $Tb_3(BDC)_{4.5}(DMF)_2(H_2O)_3\cdot(DMF)(H_2O)$ (JUC-30a) and $Ln_3(BDC)_{4.5}(DMF)_2(H_2O)_3\cdot(DMF)(C_2H_5OH)_{0.5}(H_2O)_{0.5}$ (Ln = Dy, Ho and Er, JUC-30(b–d)) by the reaction of the lanthanide metal ion ($Ln^{3+}$) with BDC and TEA [63]. They are extremely similar in structure and crystallized in the triclinic space group *P*-1. An edge-sharing

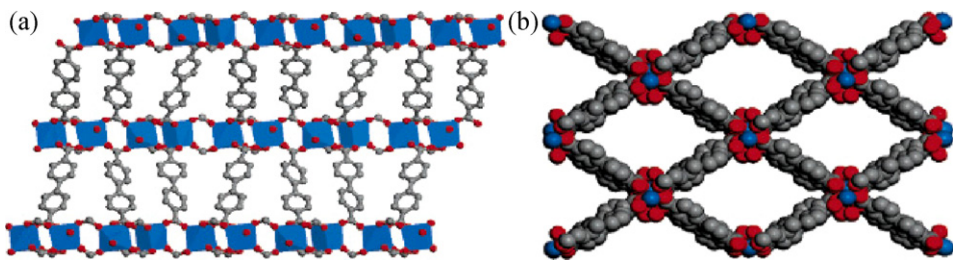


**Fig. 18.** Crystal structure of JUC-28a, containing (a) infinite —Tb–O–C–O–Tb— inorganic chains viewed along the [0 1 0] direction and (b) 1D large channels viewed along the [0 0 1] direction (figure was reproduced from Ref. [62], with permission of the copyright holders).

metallic dimer and 4 metallic monomers assemble with 18 carboxylate groups to form discrete inorganic rod-shaped building units [$Ln_6(CO_2)_{18}$], which link to each other through phenyl groups to lead to three-dimensional open frameworks with approximately 4 Å × 6 Å rhombic channels along the [0 −1 1] direction (Fig. 19). A water sorption isotherm proves that guest molecules in the framework of JUC-30a can be removed to create permanent microporosity and about four water molecules per formula unit can be adsorbed into the micropores. These complexes exhibit blue fluorescence, and JUC-30a shows a $Tb^{3+}$ characteristic emission in the range of 450–650 nm.

Subsequently, a series of rare earth MOFs, M(BTC)(DMF)(DMSO) (M = Tb, Ho, Er, Yb and Y, JUC-31(a–e)), with zeolite ABW topology were crystallized under mild conditions [64]. These compounds exhibit the same 3D architecture and crystallize in the monoclinic symmetry space group $P2_1/n$. Their structures are built up from inorganic 4-connected building units ($M(CO_2)_4$) and organic 4-connected building units (BTC ligands). These building units link to each other to generate about 5 Å × 8 Å channels along the [1 0 0] direction (Fig. 20). The luminescent and magnetic properties of these compounds have been investigated.

Additionally, we have also prepared a lanthanide metal–organic framework, Dy(BTC)($H_2O$)·DMF (JUC-32), synthesized under mild conditions [65]. As shown in Fig. 21, the framework contains approximately 6 Å × 6 Å circular channels along the [0 0 1] direction to which the coordination water molecules point. In this structure, terminal water molecules could be removed after calcination at 300 °C to lead to available Lewis-acid metal sites. The sample after removal the guest molecule and terminal coordinated molecule shows high surface area, 655 $m^2\ g^{-1}$, and high capacity for storage of hydrogen and carbon dioxide.

Recently, we synthesized one lanthanum metal–organic framework, $La_2(QS)_3(H_2O)_3{\cdot}3$ (DMA) (JUC-71), synthesized under solvothermal conditions. Viewed from [0 0 1] direction, there are non-interpenetrating honeycombed one-dimensional channels with 7.5 Å × 7.5 Å taking into account the van der Waals radii of the atoms (Fig. 22). It is outstanding that this compound is a hydrothermally ultra-stable microporous MOF. The hydrothermal stability was examined by suspending the as-synthesized sample in 100 °C water and after 7 days, the sample had retained its crystallinity. The nitrogen adsorption study shows it has a high surface area, 1197 $m^2\ g^{-1}$ after removal of the guest molecules [66].

### 2.8. Fabrication of MOF membrane

Porous solid based films, namely inorganic zeolite membranes, are efficient for gas separation [67,68]. Nevertheless difficulties to functionalize the pores and thus control their flux properties have limited their universal application. The versatility of MOFs may allow these limitations to be overcome and provide new routes to the synthesis of tunable supports for gas separation. However the preparation of thin films in this field remains an important challenge. At present, little progress has been made to construct MOF-based films.

Recently we have successfully synthesized the copper net supported $Cu_3(BTC)_2$ membrane ($Cu_3(BTC)_2$, HKUST-1) by means of a "twin copper source" technique (Fig. 23). Compared with the conventional zeolite membranes, the copper net supported $Cu_3(BTC)_2$ membrane exhibits a higher permeation flux and excellent permeation selectivity for $H_2$ [69]. Such characteristics of the copper net supported $Cu_3(BTC)_2$ membrane offer great potential toward applications such as separating, recycling, and reusing $H_2$ exhausted from steam reforming of natural gas.

## 3. Multifunctional properties

As a new kind of porous material, MOFs manifest more attractive potential applications compared to traditional porous materials, which are mostly due to the possibilities for fine-tuning and modification of their pore structures and properties like pore dimensions, shapes, sizes, and pore surface properties. Most of MOFs have three-dimensional structures incorporating uniform pores and a network of channels. These pores and channels are often filled with terminal and guest species, usually solvent, organic amine

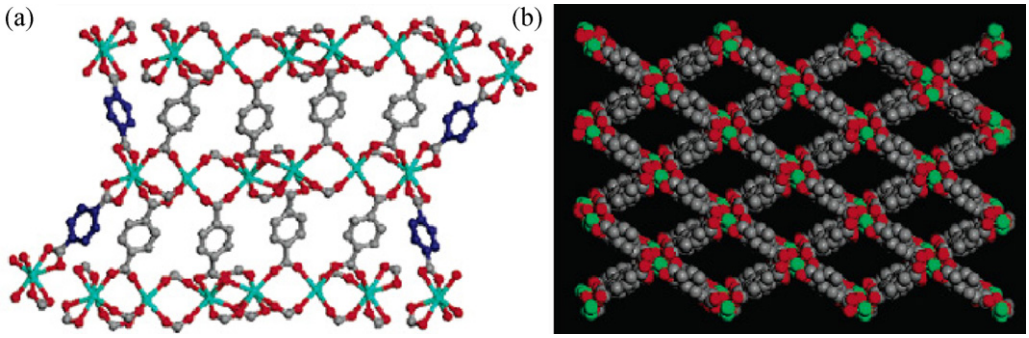


**Fig. 19.** The structure of JUC-30a. (a) BDC ligands whose carboxylate groups adopted di-monodatate and chelating/bridging bidentate coordination modes are similar to the "linkers" of the infinite rod-shaped SBUs, and those adopting a chelating bidentate mode like the "struts" to connect the hexameric units. (b) One-dimensional channels viewed along the [0 1 1] direction (figure was reproduced from Ref. [63], with permission of the copyright holders).

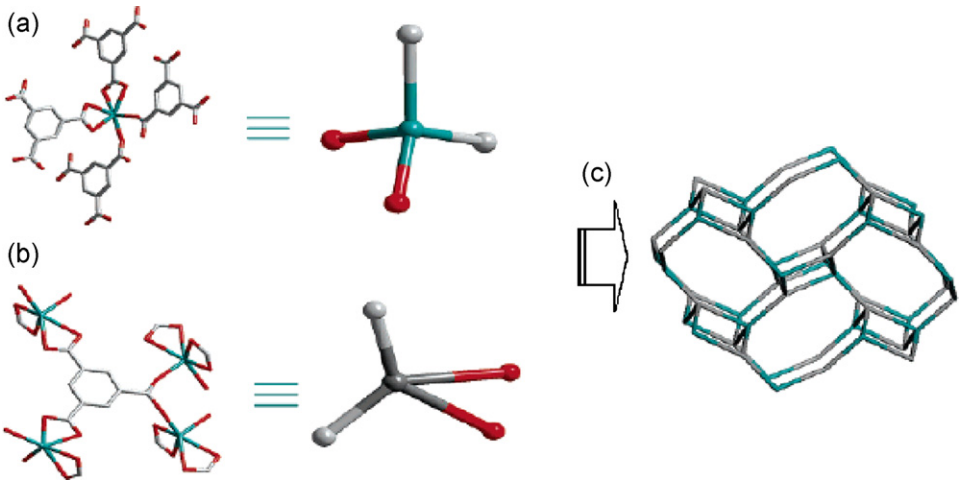


**Fig. 20.** The structure of JUC-31a. (a) Inorganic four-connected node containing one metal center connected with four BTC ligands and (b) an organic four-connected node presenting one phenyl group linked with four mental centers which link to each other to produce (c) a zeolite ABW topology (figure was reproduced from Ref. [64], with permission of the copyright holders).

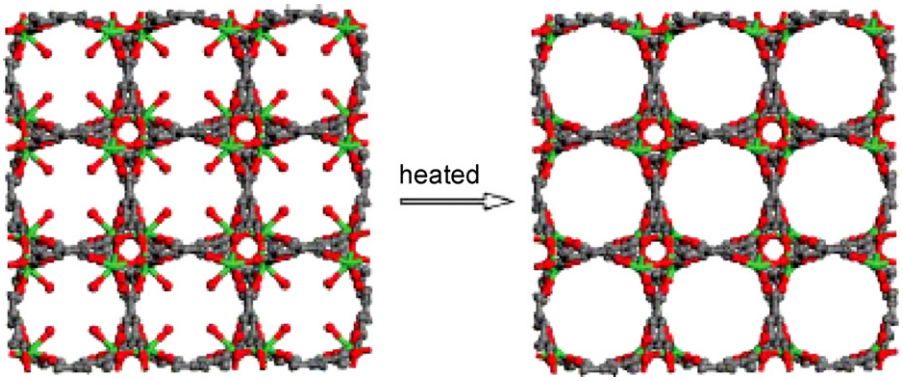


**Fig. 21.** Left, a three-dimensional network of JUC-32 with approximately 7 Å × 7 Å circular channels along [0 0 1] direction to which the coordinated water molecules point, which could be removed through heating the sample at 300 °C to yield micropores (right) (figure was reproduced from Ref. [65], with permission of the copyright holders).

base, sometimes ions from synthesis. Removal of these guests often leads to framework collapse; however, in many cases, framework integrity is preserved, and these voids remain and other guest molecules can then be adsorbed onto this porous structure. In the structure of MOF, SBUs decorate the nodes and expand the inorganic topology, which gives them exceptionally high porosity. MOFs also have uniform and tunable pore size, due to their crystalline state. Through removal of the terminal ligands (such as aqua and pyridine) with introduction of organic groups, two kinds of well-defined molecular adsorption sites in MOF structures, unsaturated metal centers (UMC) and guest-accessible functional organic sites (FOS), can be reached [70]. For example, by removing the terminal aqua of

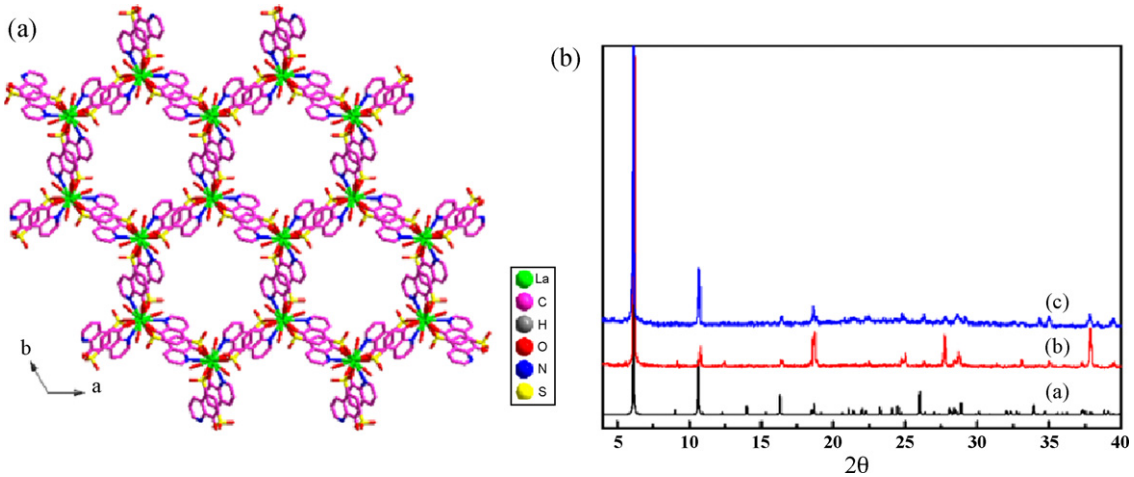


**Fig. 22.** (a) A 3D network of JUC-71 with approximately 7.5 Å × 7.5 Å honeycombed channels along [0 0 1] direction; (b) Power X-ray diffraction patterns of compound, simulated from the crystal data (a, black); as-synthesized (b, red); upon immerging in 100 °C water for 7 days (c, blue) (figure was reproduced from Ref. [66], with permission of the copyright holders).

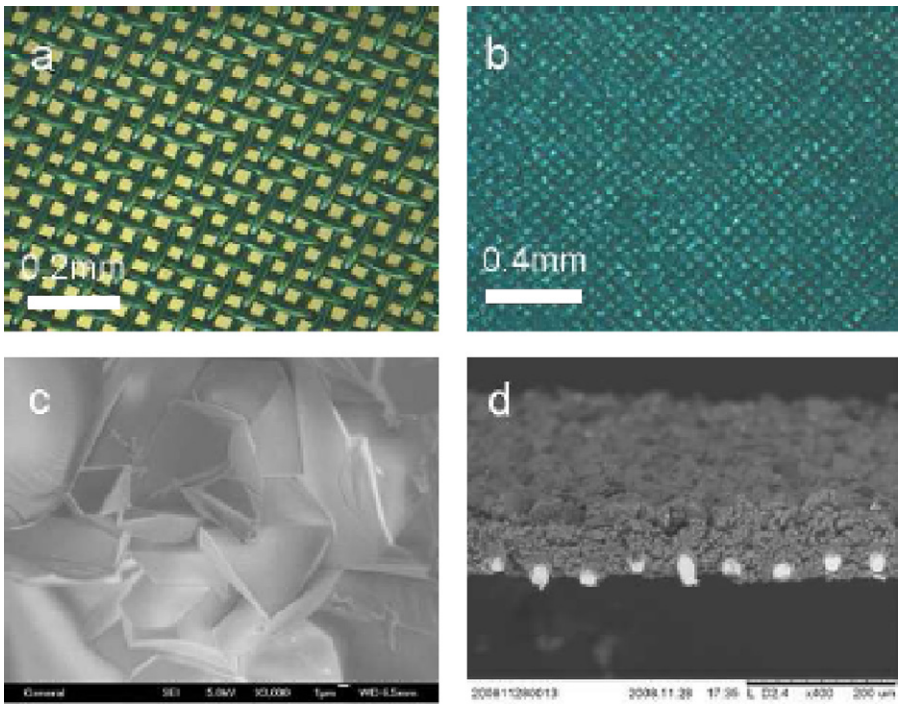


**Fig. 23.** Optic micrographs of (a) the copper net and (b) the netsupported $Cu_3(BTC)_2$ membrane; SEM image of (c) the surface and (d) cross-section of the membrane (figure adapted from Ref. [69]).

paddle-wheel SBUs and using the adip ligand with the anthracene rings, Zhou et al. obtain a MOF with high excess hydrogen adsorption capacity of 2.70 wt% at 77 K, 760 Torr, as well as high hydrogen affinity of 8.6 KJ/mol at low $H_2$ coverage. These porous features of MOFs result in a more effective and wide range of applications.

### 3.1. Energy storage

With the improvement of living standards and the growth of population, global energy consumption is expected to increase steadily over the next 50 years. In the meanwhile, the escalating atmospheric level of carbon dioxide will irreparably damage the global ecosystem. These challenges result in the expansion of research into more secure and diversified energy sources. Among various alternative fuels, hydrogen and methane have been recognized as ideal energy carriers and have the potential to reduce our dependence on fossil fuels, due to their clean combustion and high heating value**.** Although methane will create $CO_2$ after burning, it is still a potential automobile fuel because it is significantly cleaner than petroleum [71]. However, hydrogen and methane are both volatile gases under ambient conditions. Effective storage and delivery of them become the key elements of the practical applications. MOF as a novel kind of porous materials with high porosity, uniform and tunable pore size, and functional pore surfaces rapidly becomes a candidate of hydrogen and methane storage materials [72].

In May 2003, Yaghi et al. reported what is believed to be the first measurements of hydrogen adsorption on $Zn_4O(BDC)_3$ (MOF-5), where $H_2BDC$ is terephthalic acid, a remarkable 4.5 wt% at 77 K and 1 atm, and 1.0 wt% at room temperature and 20 bar. In 2006, they reported another highly porous MOF, $Zn_4O(BTB)_2$ (MOF-177), reaches an even higher total gravimetric uptake, 7.5 wt% at 77 K and 78 bar (Fig. 24) [73,74]. Since 2003, at least 150 unique MOFs have been evaluated for their ability to store hydrogen.

Coupled with measurements of porosity based on nitrogen adsorption, many methods have been developed to obtain a detailed understanding of the localizations of $H_2$ within MOFs. Neutron diffraction, inelastic neutron scattering, and infrared spectroscopy have been used to explore the site-specific interactions of hydrogen within a framework and the energies of those binding events [75–77]. Computational studies, involving both electronic structure methods (ab initio and DFT) and molecular mechanics (Grand Canonical Monte Carlo methods), have added insight to these remarkable materials and the mechanisms of hydrogen adsorption [78].

MOFs are high pure crystalline and physisorption-based material, and easy to synthesize. They do not have the problems that other hydrogen storage materials such as carbon-based materials and solid metal hydrides have, like the higher temperature needed for desorption of hydrogen, low gravimetric hydrogen content, problem associated with their regenerations, costs, unfavorable kinetics requiring heating cycles, and susceptibility to contamination by impurities. However, MOFs show exceptional $H_2$ uptake by mass but are also characterized by very weak $H_2$ adsorption energies (typically 4–10 kJ/mol), such that cryogenic temperatures are required to observe significant $H_2$ storage. Several design principles have been proposed to increase the hydrogen storage properties in their frameworks [79].

(1) A high framework porosity is necessary for high hydrogen saturation uptake. Some examples, at high pressures and low temperature, 6.01 wt% for MIL-101 and 6.7 wt% for IRMOF-20 at 77 K of hydrogen were adsorbed. Both of the compounds have 80% free volume [80,81].
(2) The enthalpy of adsorption is also greatly dependent on the size of the pore. Narrow pores actually take up hydrogen more effectively than very large ones. Hence, catenation and interpenetration networks are designed for hydrogen storage. Zhou et al. reported the hydrogen uptake of a couple of isostructural compounds, catenated PCN-6 and non-catenated PCN-6′. They found that the hydrogen storage in catenated PCN-6 is more effective than that in non-catenated PCN-6′ [82]. In 2008, we reported JUC-61 with a triply interpenetrated primitive cubic net [83]. Of most interest is the significantly high

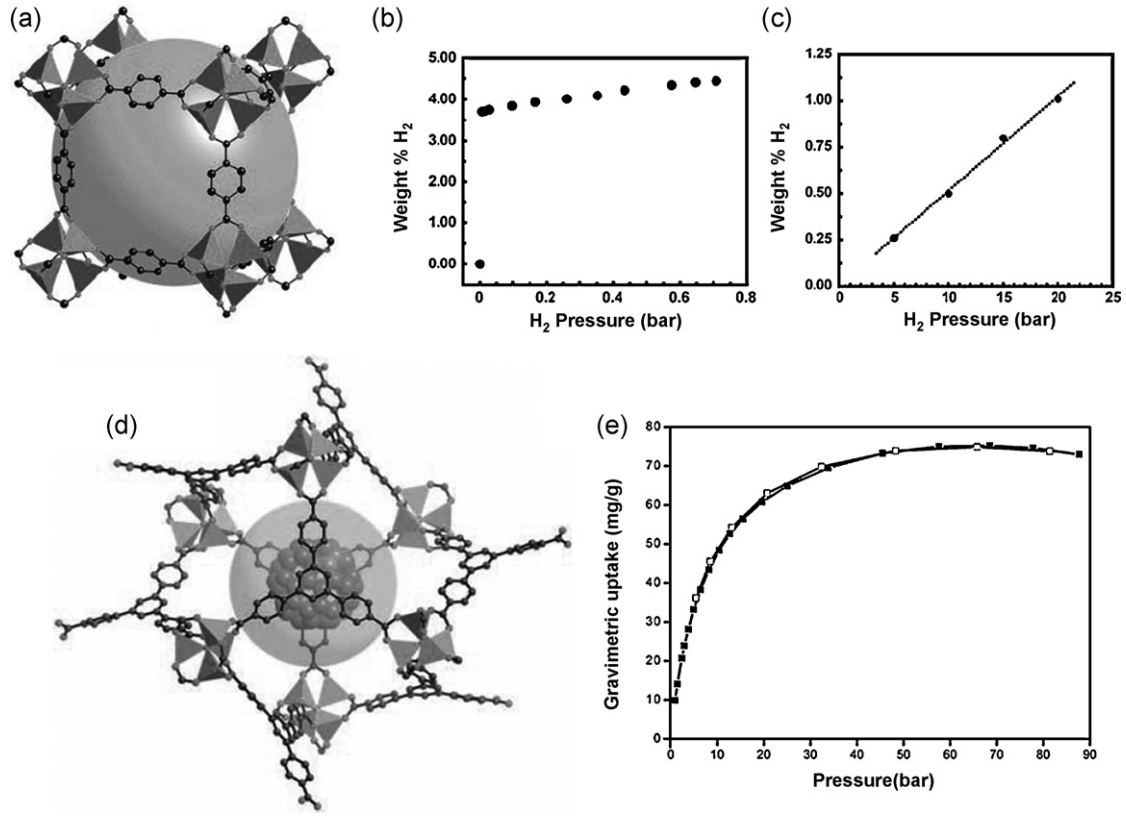


**Fig. 24.** Single-crystal X-ray structure of MOF-5 (a) and hydrogen gas-sorption isotherm for MOF-5 at 78 K (b) and 298 K (c). Single-crystal X-ray structure of MOF-177 (d) and hydrogen gas-sorption isotherm for MOF-177 at 78 K and high pressure (e) (figure was reproduced from Ref. [73,74], with permission of the copyright holders).

hydrogen uptake of 1.28 wt% [142.6 $cm^3\,g^{-1}$ (STP)] at 1 atm for such low porous MOFs. The density for adsorbed $H_2$ of JUC-61 is 0.0674 g/$cm^3$ based on the measured pore volume (0.19 $cm^3$/g), thus the fraction of the pore volume filled by liquid $H_2$ ($\rho H_2$ = 0.0708 g/$cm^3$) is 95.2% at 1 atm and 77 K, suggesting that $H_2$ almost entirely fills the pores of JUC-61. At low coverage, JUC-61 exhibits a moderate high $H_2$ adsorption enthalpy of 7.85 kJ/mol, which is higher than that of MOF-5 (5.2 kJ/mol), HKUST-1 (6.6 kJ/mol) or Prussian blue (7.4 kJ/mol) (Fig. 25).

(3) Partial charges, either positive or negative, on the MOF surface can provide a means of strengthening the binding of $H_2$ through dipole-induced dipole interactions. Especially, the introduction of open metal sites into MOF is considered one of the most effective means of increasing the $H_2$ adsorption enthalpy [84]. Long et al. reported the hydrogen storage in a microporous MOF, $[Mn(DMF)_6]_3[(Mn_4Cl)_3(BTT)_8(H_2O)_{12}]_2{\cdot}42(DMF){\cdot}11(H_2O){\cdot}20(CH_3OH)$ with exposed $Mn^{2+}$ coordination sites [85]. The desolvated form of this compound, $Mn_3[(Mn_4Cl)_3(BTT)_8(CH_3OH)_{10}]_2$ shows a total $H_2$ uptake of 6.9 wt% at 77 K and 90 bar, and exhibits a maximum isosteric heat of adsorption of 10.1 kJ/mol [Fig. 33(a) and (b)]. They also reported the isostructural MOF, $HCu[(Cu_4Cl)_3(BTT)_8]{\cdot}3.5(HCl)$, with exposed $Cu^{2+}$ coordination sites and observed the $Cu^{2+}$–$H_2$ interactions via powder neutron diffraction experiments [86]. In 2008, we reported a 3D MOF, JUC-62, with NbO topology and exposed $Cu^{2+}$ coordination sites

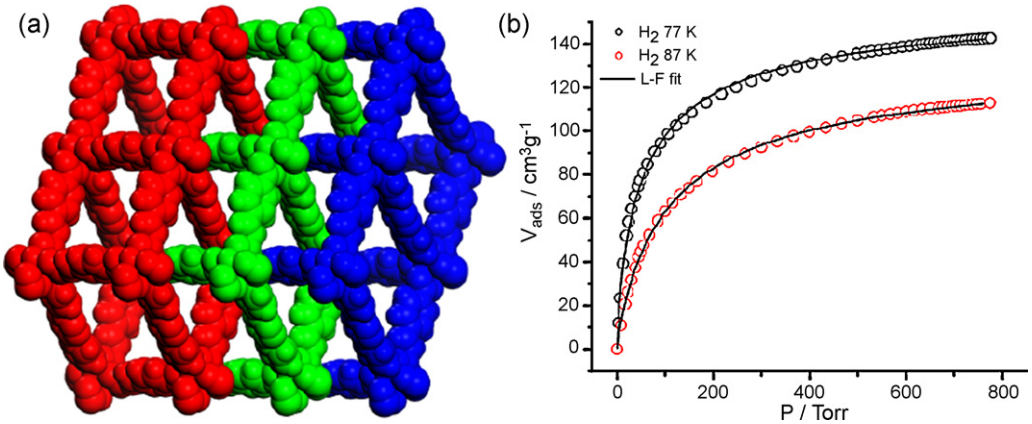


**Fig. 25.** (a) Triply interpenetrated structure of JUC-61 showing a 1D triangular channel of 3.7 Å viewed along the rectangular diagonal of the cubic lattice; (b) $H_2$ adsorption isotherms for JUC-61 in liquid nitrogen (77 K, black circles) and liquid argon (87 K, red circles). Solid lines correspond to Langmuir–Freundlich fits to the experimental data (figure was reproduced from Ref. [83], with permission of the copyright holders).

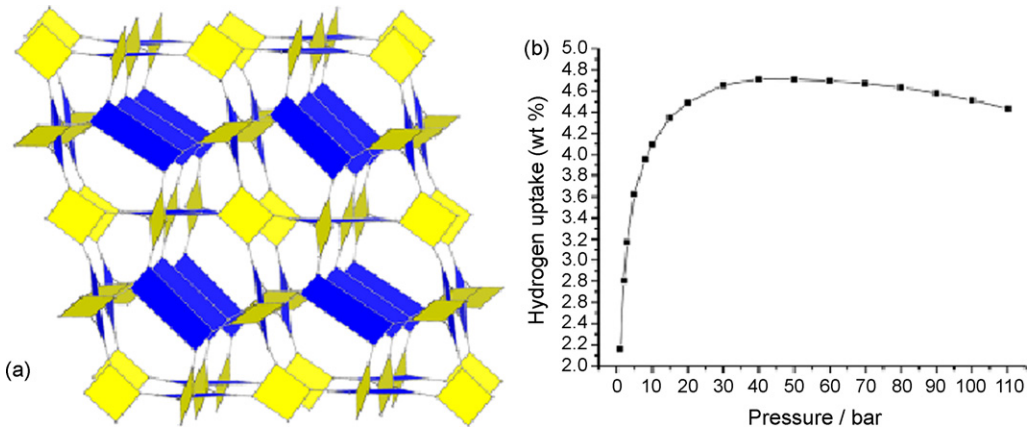


**Fig. 26.** (a) The NbO network of JUC-62; (b) high-pressure hydrogen adsorption isotherm for the activated JUC-62 at 77 K (figure was reproduced from Ref. [87], with permission of the copyright holders).

[87]. The activated JUC-62 reveals a type I profile which is saturated at 40 bar with a hydrogen uptake of about 4.71 wt%, which corresponds to a $H_2$ storage capacity of 38.4 g/L (Fig. 26).

In addition to hydrogen, methane is also an alternative fuel to replace gasoline and diesel fuels in vehicular applications. The research based on MOFs as methane storage materials has attracted more and more attention. Actually, some strategies used to achieve high hydrogen storage properties can be shared with methane storage research, like high porosity and appropriate pore size. In 1999, Kitagawa et al. reported the methane adsorption capabilities of three pillared-layer structures. The highest methane adsorption reaches 2.9 mmol/g at ambient temperature and 36 atm [88]. They also reported a highly porous MOF in 2000, in which the methane adsorption capacities reached 6.9 mmol/g at ambient temperature and 36 atm. This is much larger than zeolite 5A (about 3.7 mmol/g) under the same conditions [89]. In 2002, Yaghi et al. reported IRMOF-n series and their methane storage capacities. One member, IRMOF-6, exhibited a high capacity for methane storage, up to 155 v(STP)/v at 35 atm and 298 K compared with 87, v/v, by zeolite 5A at same conditions [18]. In 2008, Zhou et al. reported a MOF, PCN-14, synthesized with a new ligand, $H_4$adip. PCN-14 exhibits an absolute methane adsorption capacity of 230 v(STP)/v (28% higher than the DOE target of 180 v(STP)/v at ambient temperatures) and heats of adsorption of methane of around 30 kJ/mol, both record highs among those reported for methane storage materials (Fig. 27) [90].

### 3.2. Separation

MOFs as porous materials allow their pore properties (e.g., pore size, pore volume and the chemical functionality of the pore walls) to be systematically tuned by the judicious choice of the metal and ligand constituents and synthesis approach, which makes these microporous materials potentially useful for molecule separation. In 2006, Li et al. reported a highly stable guest-free microporous MOF, Zn(tbip), which contains close-packed 1D channels and all the methyl groups of the ligand protruding into the channels [91]. The special channel surface causes the framework to be very hydrophobic, and the effective channels of 4.5 Å allow it to adsorb normal paraffins, methanol, and dimethyl ether but to exclude aromatics. In the same year, they reported another hydrophobic microporous material, Cu(hfipbb)($H_2$hfipbb)$_{0.5}$ [92]. This compound contains special channels consisted of alternating oval-shaped large chambers and narrow windows. This feature of these micro-channels allows their shape and size selectivity for hydrocarbon sorption. They also calculated the gas-sorption simulations using the sorption module of the Cerius$^2$ program. The calculated results coincide well with those of the experimental adsorption measurements. More excitingly, for the first time, Chen et al. demonstrated the application of a microporous MOF, MOF-508, in the GC separation of alkanes based on the size and shape-selective matching [93]. In 2007, Zhou et al. reported an interesting graphitic MOF structure, MAMS-1, generated by packing of trilayers [94]. Packing of the trilayers generates hydrophobic gas-storage chambers, which are not accessible without activation. Most interestingly, temperature can be used to tune the gates of MAMS-1 to open linearly, thus giving rise to an unprecedented molecular sieve with an adjustable mesh that can separate any two gases with kinetic diameters in the range of 2.9–5.0 Å.

One of the advantages of MOFs for molecular separation is the functionality of their pore surface. The separation of small molecule $C_2H_2$ from a mixture containing carbon dioxide is very important for industry. However, because $C_2H_2$ and $CO_2$ are similar to one another in equilibrium sorption parameters, related physicochemical properties, and molecular size and shape, the separation is not easy. In 2005, Kitagawa et al. reported high levels of selective sorption of acetylene molecules as compared to carbon dioxide, onto the functionalized surface of a MOF, $Cu_2$(pzdc)$_2$(pyz) [95]. They also found the acetylene molecules are held at a periodic distance from one another by hydrogen bonding between two non-coordinated oxygen atoms in the nanoscale pore wall of the framework and the two hydrogen atoms of the acetylene molecule via MEM electron density views (Fig. 28).

JUC-61 is a triply interpenetrated structure, which has a restricted pore size for gas separation [83]. When methanol-exchanged JUC-61 was activated at 75 °C under high vacuum overnight, the activated phase JUC-61a took up quite a large amount of hydrogen (117 cm$^3$/g) but a negligible amount of nitrogen (Fig. 29a), underlying the separation capacity of JUC-61a for $H_2/N_2$ separation. JUC-61a was further activated at a higher temperature of 120 °C under high vacuum overnight to form JUC-61b in which all the guest solvent molecules were completely removed. JUC-61b also exhibits selective sorption of $CO_2$ (3.3 Å) over $CH_4$ (3.8 Å) at 195 K (Fig. 29b).

Enantioselective separation is especially important for the chemical and pharmaceutical industries. However, it's very difficult to achieve enantioselective separation using traditional porous materials. In 2000, Kim et al. reported a family of homochiral porous MOFs, D/L-POST-1 [54]. Owing to the chiral environment of the channels, L-POST-1 allows the enantioselective inclusion of metal complexes, [Ru(2,2′-bipy)$_3$]Cl$_2$. Nuclear magnetic resonance (NMR), ultraviolet–visible and circular dichroism measurements showed that 80% of the exchangeable protons are exchanged with [Ru(2,2′-bipy)$_3$]$^{2+}$ with 66% enantiomeric excess in favor of

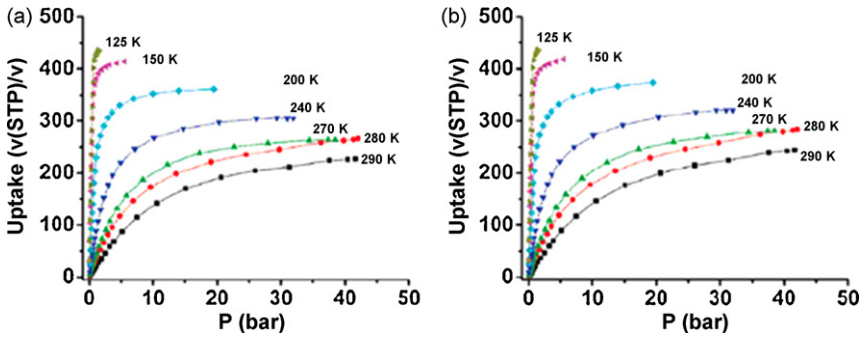


**Fig. 27.** High-pressure methane sorption isotherms at various temperatures of PCN-14. (a) Excess adsorption; (b) absolute adsorption (figure was reproduced from Ref. [90], with permission of the copyright holders).

the D form. In 2006, they utilized a new approach, which links homochiral SBUs formed by metal ions and available homochiral organic ligand L-lactic acid, and synthesized a new homochiral MOF, $[Zn_2(BDC)(L\text{-lac})(DMF)]\cdot(DMF)$, in a one-pot reaction [52]. This 3D structure has size-selective and enantioselective sorption abilities of several substituted thioether oxides. Rosseinsky et al. are also interested in the synthesis of chiral porous MOFs and their enantioselective separation properties. In 2004, they reported two isostructural homochiral MOFs, $M_3(BTC)_2$, where M is $Ni^{2+}$ or $Co^{2+}$ [96]. The structure belongs to the chiral (10,3)-a topology. They found the enantioselective sorption of some chiral guest species, $E_3HB$, the terpenes menthone, fenchone and the aromatic diol binaphthol, by the framework. In 2006, they reported a family of nanoporous materials based on an amino acid backbone, $[Ni_2(D/L\text{-asp})_2(bipy)]\cdot 1.28CH_3OH\cdot 0.72H_2O$ [97]. The desolvated sample retains its open-framework structure and shows enantioselective sorption by using a library of small chiral molecules. A geometry-dependent interaction between the framework and the guests is also found by computational approaches.

### 3.3. Catalysis

Over the past 10 years, the use of MOFs as solid catalysts is particularly interesting because the pore size and functionality of the framework can be adjusted over a wide range for a variety of catalytic reactions. Although a large number of different MOFs are known, only a few of them have been tested in catalytic reactions so far. It is still an enormous challenge to find out whether the metal centers, the ligands or functionalized ligands, or even metal–ligand interactions or differences in particle size, can cause unusual catalytic properties.

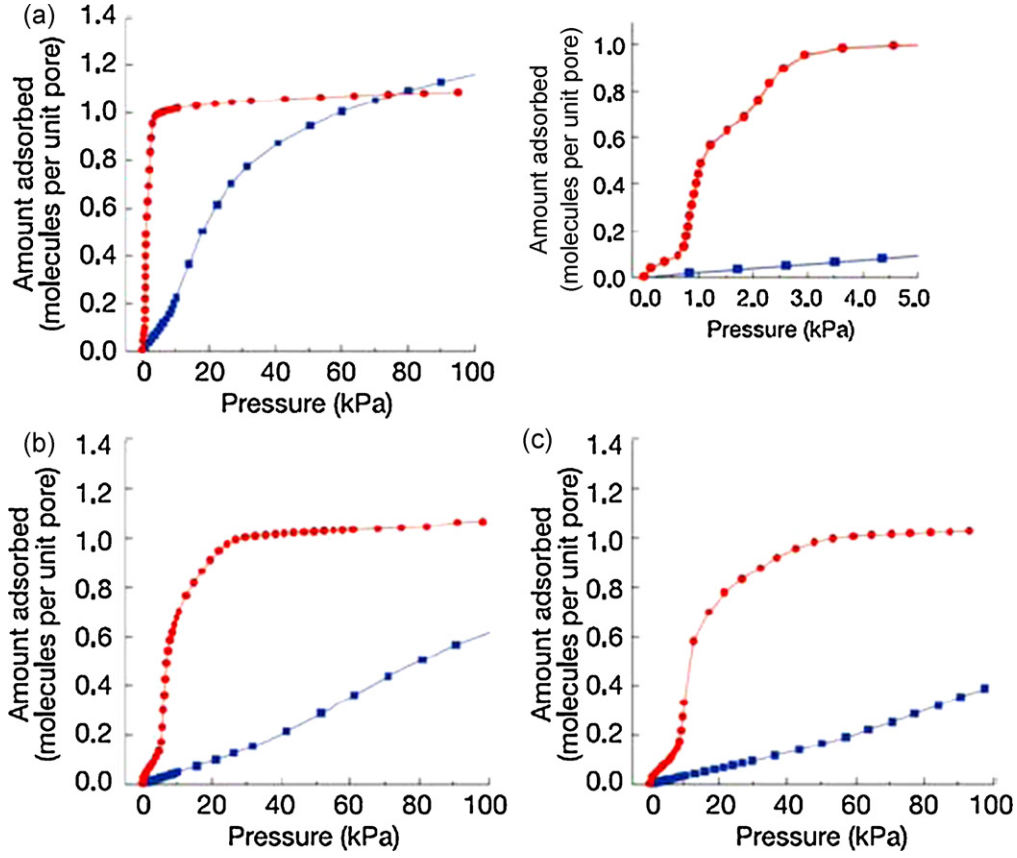


**Fig. 28.** Adsorption isotherms for $C_2H_2$ (red circles) and $CO_2$ (blue squares) on $Cu_2(pzdc)_2(pyz)$. The pressure range is from $10^{-4}$ to 100 kPa and the temperatures are at 270 K (a; the inset shows the lower $P/P_0$ region), 300 K (b) and 310 K (c) (figure was reproduced from Ref. [95], with permission of the copyright holders).

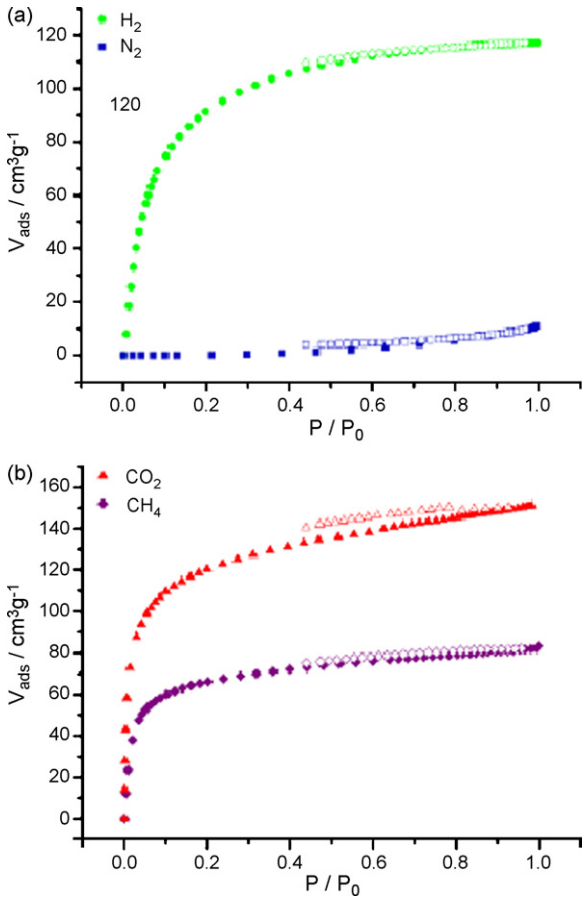


**Fig. 29.** (a) Gas-sorption isotherms of JUC-61a at 77 K (hydrogen, green/circle; nitrogen, blue/square); (b) Gas-sorption isotherms of JUC-61b at 195 K (carbon dioxide, red/triangle; methane, purple/rhombus; solid and open shapes represent adsorption and desorption, respectively) (figure was reproduced from Ref. [83], with permission of the copyright holders).

Lin et al. have reported a homochiral porous MOFs by using axially chiral bridging ligand (*R*)-DDBB, which contains the bipyridyl primary functionality and orthogonal chiral 2,2′-dihydroxy secondary functionality [55]. In this structure, each Cd(II) center is coordinated by two pyridyl groups of the ligands and connects adjacent 1D $[Cd(\mu\text{-}Cl)_2]_n$ SBUs to form a non-interpenetrating 3D network with very large chiral channels of ~1.6 × 1.8 nm cross-section along the *a*-axis. Subsequently, they treated this compound with excess $Ti(O^iPr)_4$ leading to an active catalyst for $ZnEt_2$ addition reactions. Specifically, the compound treated with $Ti(O^iPr)_4$ catalyzes the addition of $ZnEt_2$ to 1-naphthaldehyde to afford (*R*)-1-(1-naphthyl)propanol with complete conversion and 93% enantiomeric excess (ee) (Fig. 30).

The embedding of Ru nanoparticles into the otherwise unchanged metal–organic framework MOF-5 was investigated by Fischer and co-workers [98]. Firstly, the well-defined inclusion compound $[Ru(cod)(cot)]_{3.5}$@MOF-5 was derived, and then hydrogenolysis to form Ru nanoparticles inside the cavities was performed, leading to a material denoted as Ru@MOF-5. Preliminary results on the catalytic activity of Ru@MOF-5 in alcohol oxidation revealed the limitations of the water-sensitive MOF-5 host material for catalytic applications of the system metal@MOF-5.

Férey and co-workers showed that the presence of chromium(III) coordinatively unsaturated metal sites (CUSs) in chromium(III) terephthalate MIL-101 with zeotypic giant pores can provide an intrinsic chelating property with electron-rich functional groups, leading to the formation of the thermally stable amine species grafted on the surface (Fig. 31) [99]. This feature offers a powerful way to selectively functionalize the unsaturated sites in MIL-101. ED and DETA can be used as new grafting agents to produce the amine-grafted MIL-101, exhibiting remarkably high activities in the Knoevenagel condensation. Additionally, palladium loaded APS-MIL-101 and ED-MIL-101 have obviously high activities during the Heck reaction at 393 K, which is the most powerful method to couple alkenes with organic moieties.

Kitagawa et al. successfully synthesized a 3D MOF functionalized with amide groups, $\{[Cd(4\text{-btapa})2(NO_3)_2]\cdot 6H_2O\cdot 2DMF\}n$, from the reaction between $Cd(NO_3)_2\cdot 4H_2O$ and a three connector-type amide ligand (4-btapa). The amide groups are ordered uniformly on the channel surfaces [70]. The compound selectively accommodated and activated guests in its channels because of the active amide groups. Knoevenagel condensation reactions of benzaldehyde with each of the active methylene compounds (malononitrile, ethyl cyanoacetate, and cyano-acetic acid *tert*-butyl ester) were catalyzed. As a result, the malononitrile was a good substrate, producing 98% conversion of the adduct, whereas the other substrates reacted negligibly. This selectivity depends on the relationship between the size of the reactants and the pore window of the host.

The catalytic activity of the sodalite-type compound $Mn_3[(Mn_4Cl)_3(BTT)_8(CH_3OH)_{10}]_2$ was investigated by Long et al. [100]. The compound is a thermally stable microporous solid exhibiting a cubic network of 7 and 10 Å pores that affords a BET surface area of 2100 $m^2/g$, and $Mn^{2+}$ ions exposed on the surface of the framework might serve as potent Lewis acids. This compound indeed catalyzes the cyanosilylation of aromatic aldehydes and ketones, as well as the more demanding Mukaiyama-aldol reaction. Moreover, in each case, a pronounced size-selectivity effect consistent with the pore dimensions is observed.

Recently, Eddaoudi and co-workers have demonstrated the utilization of In-HImDC-based *rho*-ZMOF as a host for large catalyti-

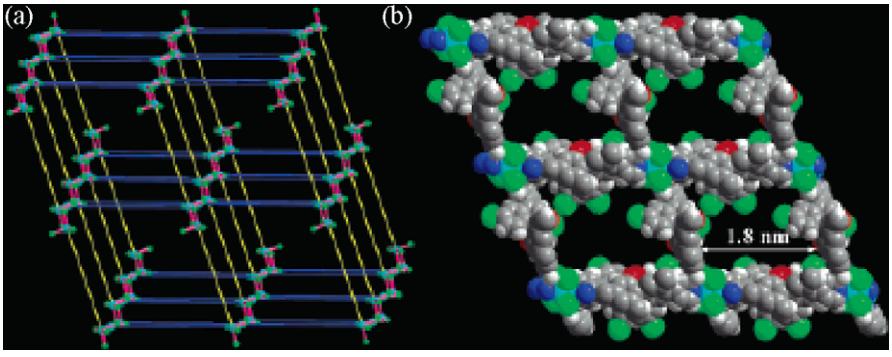


**Fig. 30.** Crystal structure of the homochiral porous MOF. (a) Schematic representation of the 3D framework as viewed slightly off the *a*-axis. (b) Space-filling model as viewed down the *a*-axis showing the large chiral 1D channels (~1.6 nm × 1.8 nm) (figure was reproduced from Ref. [55], with permission of the copyright holders).

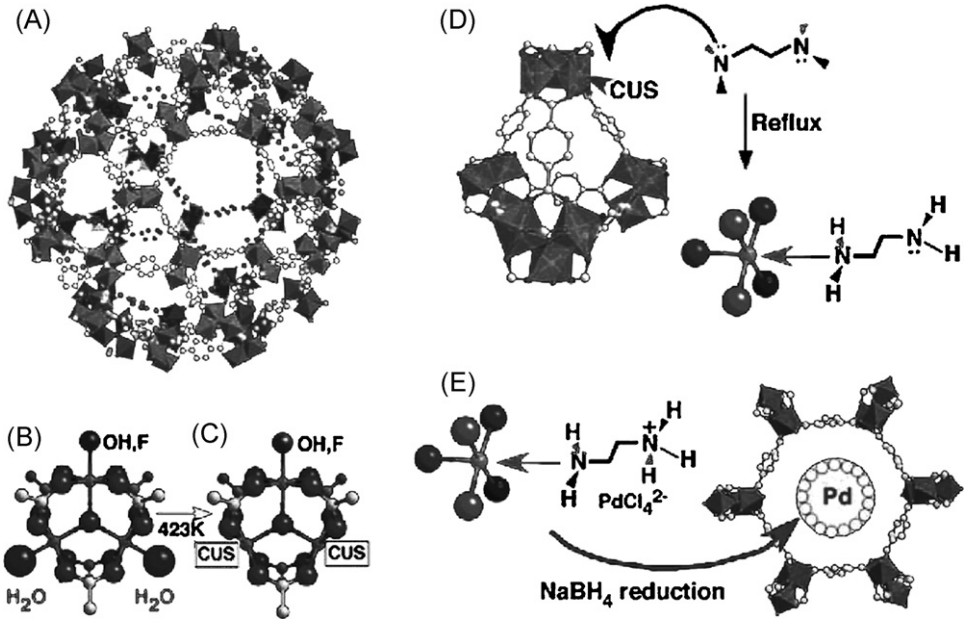


**Fig. 31.** Site-selective functionalization of MIL-101 with unsaturated metal sites: (a) perspective view of the mesoporous cage of MIL-101 with hexagonal windows; (b and c) evolution of coordinatively unsaturated sites from chromium trimers in mesoporous cages of MIL-101 after vacuum treatment at 423 K for 12 h; (d) surface functionalization of the dehydrated MIL-101 through selective grafting of amine molecules (i.e. ethylenediamine) onto coordinatively unsaturated sites; (e) selective encapsulation of noble metals in the amine-grafted MIL-101 via a three-step process (figure was reproduced from Ref. [98], with permission of the copyright holders).

cally active molecules, specifically metalloporphyrins, and its effect on the enhancement of catalytic activity [101]. To produce a versatile platform, they encapsulated the free-base porphyrin, which was readily metallated by various transition-metal ions to produce a wide range of encapsulated metalloporphyrins. To assess catalytic activity, hydrocarbon oxidation was performed in the presence of Mn-RTMPyP, which was explored as a catalyst for cyclohexane oxidation.

### 3.4. Sensors

MOFs that have magnetic or luminescence properties together with size- or shape-selective sorption can be potentially applied in sensor devices. In 2003, Veciana et al. reported an open-framework $Cu_3(PTMTC)_2(py)_6(CH_3CH_2OH)_2(H_2O)$ (MOROF-1), MOROF-1 combines very large pores (2.8–3.1 nm) with bulk magnetic ordering [102]. This compound shows a reversible and highly selective solvent-induced 'shrinking–breathing' process that strongly influences the magnetic properties of the material. This magnetic sponge-like behavior could be a route towards magnetic solvent sensors. However, the guest-dependent magnetic properties of MOROF-1 and most porous magnets are due to changes in the metal coordination environment induced by guest adsorption or substitution rather than to magnetic exchange with a paramagnetic adsorbate. In 2008, Long et al. reported two Prussian blue analogues $CsNi[Cr(CN)_6]$ and $Cr_3[Cr(CN)_6]_2$, which are microporous magnets and exhibit changes in their magnetic properties upon adsorption of $O_2$ but not $N_2$, indicating the presence of magnetic exchange coupling between the $O_2$ guest molecules and the frameworks (Fig. 32) [103].

Studies of MOFs as potential sensors with luminescent properties are more popular. Luminescent networks can be prepared by utilizing luminescent organic building blocks and/or luminescent metal building blocks, or by utilizing the ligand-to-metal charge transfer.

The presence of lanthanide centers can provide luminescence. In 1999, Yaghi et al. reported a condensed lanthanide coordination solid, $Tb_2(BDC)_3\cdot(H_2O)_4$, which has water as terminal ligands in the structure [104]. Upon removal of the terminal water by heating, a microporous MOF $Tb_2(BDC)_3$ which has 1D channels and

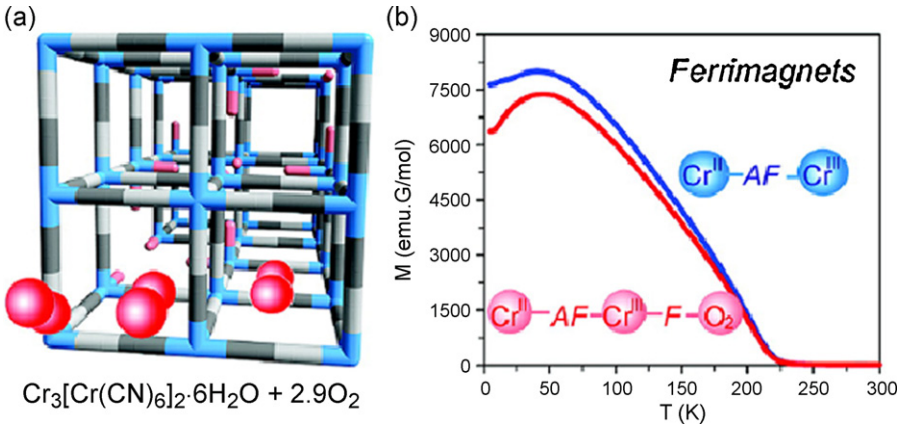


**Fig. 32.** (a) Crystal structure of $Cr_3[Cr(CN)_6]_2\cdot 6H_2O$. (b) Magnetic behavior of $Cr_3[Cr(CN)_6]_2\cdot 6H_2O$ (blue) and $Cr_3[Cr(CN)_6]_2\cdot 6H_2O$ sealed in a quartz tube containing 2.9 molecules of $O_2$ per formula unit (red) (figure was reproduced from Ref. [103], with permission of the copyright holders).

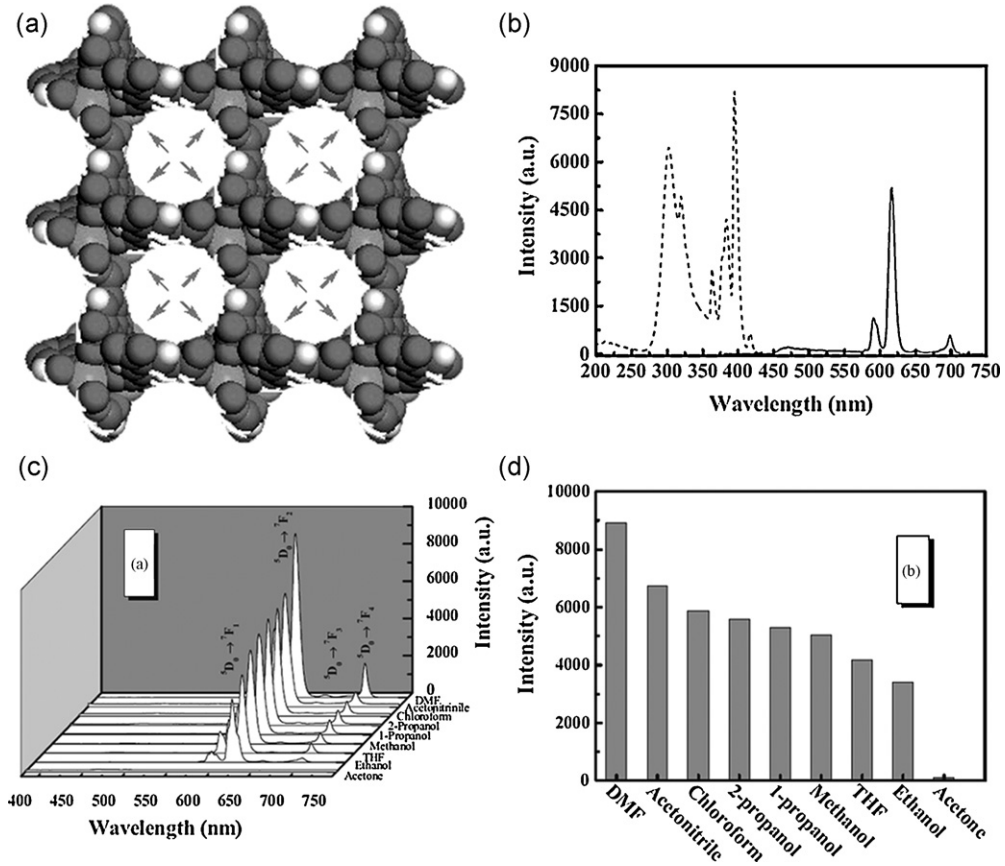


**Fig. 33.** (a) X-ray structure of Eu(BTC)($H_2O$). (b) The excitation (dotted line) and PL spectrum (solid line) of solid of Eu(BTC). (c) PL spectra of Eu(BTC) introduced into various pure solvents. (d) The $^5D_0 \rightarrow {}^7F_2$ transition intensities of Eu(BTC) introduced into various pure solvents when excited at 285 nm (figure was reproduced from Ref. [105], with permission of the copyright holders).

accessible metal sites in its channels, is achieved. The networks give different luminescence spectra depending on the presence or absence, or nature of the guest molecules which could be potential luminescent probes for the assay of small molecules. In 2007, Chen et al. reported a microporous network [Eu(BTC)($H_2O$)]·1.5$H_2O$ [105]. This compound is isostructural with MOF-76, which has 1D channels of about 6.6 Å × 6.6 Å along the c axis. The channels are filled with coordinating and free water molecules. After activation, accessible metal sites can be achieved, which is very significant for the sensor function and sensitivity of the luminescence. The fluorescence properties of the compound Eu(BTC) vary in different solvent emulsions, which allow the potential applications as a sensing material of small molecules. DMF and acetone exhibit the most significant enhancing and quenching effects, respectively. The fluorescence intensity gradually increases with the addition of DMF solvent, while decreases with the addition of acetone solvent (Fig. 33).

In 2005, Suh et al. reported $Zn_4O(NTB)_2$·3DEF·EtOH and its desolvated solid $Zn_4O(NTB)_2$ [5]. The network solid and its guest removed sample show intense photoluminescence at $\lambda_{max}$ = 433 nm and $\lambda_{max}$ = 463 nm upon photoexcitation at 340 nm, respectively, which is attributed to the absence and presence of

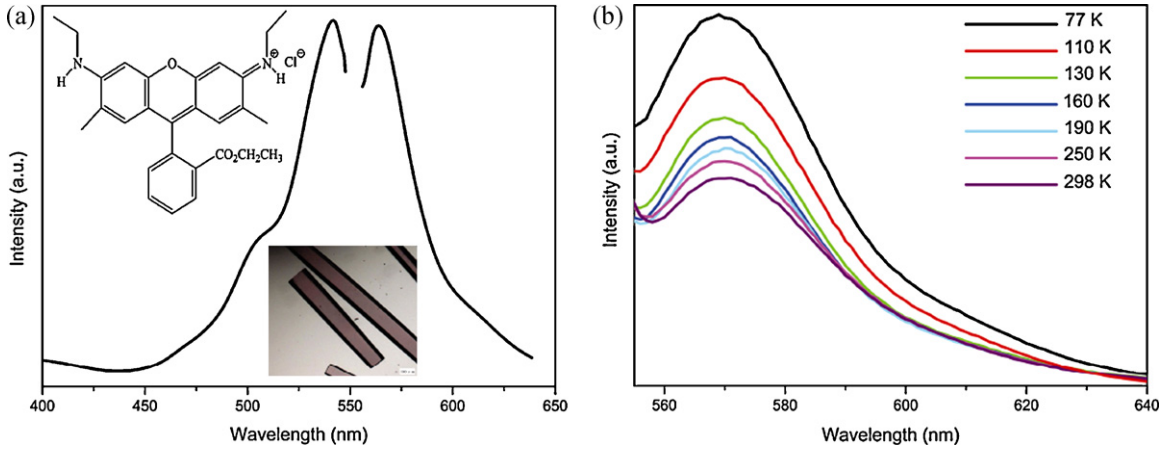


**Fig. 34.** Fluorescence spectra of JUC-48·Rh6G (a) at room temperature and (b) at different temperature. Inset: the structure of Rh6G and optical microscope image of JUC-48·Rh6G (figure was reproduced from Ref. [20], with permission of the copyright holders).

π–π interactions between the interpenetrated nets of the host. The networks with different guests exhibit guest-dependent blue photoluminescence ($\lambda_{max}$ depending on different guests), depending on the guest identity. The respective $\lambda_{max}$ of the luminescence band appears at different wavelengths when desolvated solid was immersed in the solvent such as pyridine, methanol, and benzene. The guest-dependent luminescence shows no relationship with the binding constant of the host with the guest. This guest-dependent luminescence property implies that the present porous material may be applied as a sensor for organic molecules.

JUC-48 was assembled with nanosized Rh6G dye molecules (Fig. 34a, inset). Rh6G is a xanthene derivative used as a gain medium in dye lasers. It exhibits strong absorption in the visible region and a very high fluorescence quantum yield. Fig. 34a shows the fluorescence spectra for JUC-48·Rh6G. Clearly, the strongest emission peak for JUC-48·Rh6G is at 563 nm with the excitation peak at 541 nm at room temperature, which is similar to the previous results obtained on Rh6G-doped mesostructured materials [106]. The emission spectra of JUC-48·Rh6G are also temperature-dependent. Fig. 34b shows the emission spectra of JUC-48·Rh6G recorded at different temperatures (298–77 K). The peak location of JUC-48·Rh6G at 563 nm remains unchanged with decreasing temperature, while the intensity of the signal is enhanced linearly, which reveals that JUC-48·Rh6G will be a potential candidate for applications in temperature-sensing devices.

## 4. Conclusions

MOFs as a new member of porous materials have recently become a topic of central importance to inorganic and materials chemistry. In this review, we have provided molecular engineering for synthesis of MOFs and their potential applications. In the area of synthesis there are general methods, such as diffusion method, hydro(solvo)thermal method, microwave and ultrasonic methods, particularly the important factor of organic template in the reaction process. Meanwhile, we have described the important zeolite topology MOFs, chiral MOFs, rare earth metals MOFs and MOFs membranes. In applications, we give an introduction including energy storage, molecular separation, catalysis and sensor. Compared with traditional porous materials, MOFs have some advantages, such as ease of synthesis, more choice of metal centers and multifunctional organic linkers, to achieve higher surface and pore volume, higher capacity for storage, and more multifunctional materials. Based on the potential advantages offered by MOFs, it is expected that the number of such porous materials, particularly those involving functional organic ligands, will grow dramatically in the near future. MOFs will provide extraordinary advantages over traditional porous materials and have an important and permanent impact on the future of porous compounds.

## Acknowledgments

This work was funded by the State Basic Research Project (2006CB806100), Outstanding Young Scientist Foundation of NSFC (20625102), NSFC (Grant nos. 20831D02, 20571030, 20531030, and 20371020) and "111" program of Ministry of Education of China and Bureau of Science & Technology of Jilin Province, China and International Cooperation Project of Ministry of Science and Technology (2007DFA40830). The results reviewed here have of course been obtained thanks to the contribution of other scientists, Dr. Qianrong Fang, Dr. Ming Xue and Dr. Fuxing Sun.

## References

[1] N.W. Ockwig, O. Delgado-Friedrichs, M. O'Keeffe, O.M. Yaghi, Acc. Chem. Res. 38 (2005) 176.
[2] S. Kitagawa, R. Kitaura, S. Noro, Angew. Chem. Int. Ed. 43 (2004) 2334.
[3] M.P. Suh, Y.E. Cheon, E.Y. Lee, Coord. Chem. Rev. 252 (2008) 1007.
[4] X.M. Zhang, Z.M. Hao, W.X. Zhang, X.M. Chen, Angew. Chem. Int. Ed. 46 (2007) 3456.
[5] E.Y. Lee, S.Y. Jang, M.P. Suh, J. Am. Chem. Soc. 127 (2005) 6374.
[6] Q. Ye, Y.M. Song, G.X. Wang, K. Chen, D.W. Fu, P.W.H. Chan, J.S. Zhu, S.D. Huang, R.G. Xiong, J. Am. Chem. Soc. 128 (2006) 6554.
[7] K.E. Drexler, Proc. Natl. Acad. Sci. U.S.A. -Phys. Sci. 78 (1981) 5275.
[8] A. Vonhippel, Science 123 (1956) 315.
[9] G. Ferey, C. Mellot-Draznieks, C. Serre, F. Millange, J. Dutour, S. Surble, I. Margiolaki, Science 309 (2005) 2040.
[10] O.M. Yaghi, M. O'Keeffe, N.W. Ockwig, H.K. Chae, M. Eddaoudi, J. Kim, Nature 423 (2003) 705.
[11] N.L. Rosi, J. Kim, M. Eddaoudi, B.L. Chen, M. O'Keeffe, O.M. Yaghi, J. Am. Chem. Soc. 127 (2005) 1504.
[12] M. Dinca, A.F. Yu, J.R. Long, J. Am. Chem. Soc. 128 (2006) 8904.
[13] B.L. Chen, N.W. Ockwig, A.R. Millward, D.S. Contreras, O.M. Yaghi, Angew. Chem. Int. Ed. 44 (2005) 4745.
[14] M. O'Keeffe, M. Eddaoudi, H.L. Li, T. Reineke, O.M. Yaghi, J. Solid State Chem. 152 (2000) 3.
[15] S. Noro, R. Kitaura, M. Kondo, S. Kitagawa, T. Ishii, H. Matsuzaka, M. Yamashita, J. Am. Chem. Soc. 124 (2002) 2568.
[16] G. Ferey, Chem. Soc. Rev. 37 (2008) 191.
[17] G. Ferey, C. Mellot-Draznieks, C. Serre, F. Millange, Acc. Chem. Res. 38 (2005) 217.
[18] M. Eddaoudi, J. Kim, N. Rosi, D. Vodak, J. Wachter, M. O'Keeffe, O.M. Yaghi, Science 295 (2002) 469.
[19] W.X. Zhang, Y.Y. Yang, S.B. Zai, S.W. Ng, X.M. Chen, Eur. J. Inorg. Chem. (2008) 679.
[20] Q.R. Fang, G.S. Zhu, Z. Jin, Y.Y. Ji, J.W. Ye, M. Xue, H. Yang, Y. Wang, S.L. Qiu, Angew. Chem. Int. Ed. 46 (2007) 6638.
[21] X. Shi, G.S. Zhu, S.L. Qiu, K.L. Huang, J.H. Yu, R.R. Xu, Angew. Chem. Int. Ed. 43 (2004) 6482.
[22] Z. Ni, R.I. Masel, J. Am. Chem. Soc. 128 (2006) 12394.
[23] Q.R. Fang, G.S. Zhu, M. Xue, J.Y. Sun, G. Tian, G. Wu, S.L. Qiu, Dalton T (2004) 2202.
[24] O.M. Yaghi, H.L. Li, T.L. Groy, J. Am. Chem. Soc. 118 (1996) 9096.
[25] Z.Q. Wang, V.C. Kravtsov, M.J. Zaworotko, Angew. Chem. Int. Ed. 44 (2005) 2877.
[26] Q.R. Fang, G.S. Zhu, M. Xue, Z.P. Wang, J.Y. Sun, S.L. Qiu, Cryst. Growth Des. 8 (2008) 319.
[27] J. Li, J. Yu, W. Yan, Y. Xu, W. Xu, S. Qiu, R. Xu, Chem. Mater. 11 (1999) 2600.
[28] R.M. Barrer, E.A.D. White, J. Chem. Soc. (1951) 1267.
[29] W.A. Dollase, C.R. Ross, Am. Mineral. 78 (1993) 627.
[30] Y.L. Liu, V.C. Kravtsov, R. Larsen, M. Eddaoudi, Chem. Commun. (2006) 1488.
[31] D.F. Sava, V.C. Kravtsov, F. Nouar, L. Wojtas, J.F. Eubank, M. Eddaoudi, J. Am. Chem. Soc. 130 (2008) 3768.
[32] Y.L. Liu, V.C. Kravtsov, M. Eddaoudi, Angew. Chem. Int. Ed. 47 (2008) 8446.
[33] X.C. Huang, Y.Y. Lin, J.P. Zhang, X.M. Chen, Angew. Chem. Int. Ed. 45 (2006) 1557.
[34] K.S. Park, Z. Ni, A.P. Cote, J.Y. Choi, R.D. Huang, F.J. Uribe-Romo, H.K. Chae, M. O'Keeffe, O.M. Yaghi, Proc. Natl. Acad. Sci. U.S.A. 103 (2006) 10186.
[35] B. Wang, A.P. Cote, H. Furukawa, M. O'Keeffe, O.M. Yaghi, Nature 453 (2008) 207.
[36] H. Hayashi, A.P. Cote, H. Furukawa, M. O'Keeffe, O.M. Yaghi, Nat. Mater. 6 (2007) 501.
[37] R. Banerjee, A. Phan, B. Wang, C. Knobler, H. Furukawa, M. O'Keeffe, O.M. Yaghi, Science 319 (2008) 939.
[38] M. Du, S.T. Chen, X.H. Bu, Cryst. Growth Des. 2 (2002) 625.
[39] Q.R. Fang, G.S. Zhu, M. Xue, J.Y. Sun, S.L. Qiu, Dalton T (2006) 2399.
[40] Q.R. Fang, G.S. Zhu, M. Xue, J.Y. Sun, Y. Wei, S.L. Qiu, R.R. Xu, Angew. Chem. Int. Ed. 44 (2005) 3845.
[41] H. Li, M. Eddaoudi, M. O'Keeffe, O.M. Yaghi, Nature 402 (1999) 276.
[42] Q.R. Fang, G.S. Zhu, Z. Jin, M. Xue, X. Wei, D.J. Wang, S.L. Qiu, Cryst. Growth Des. 7 (2007) 1035.
[43] Q.R. Fang, G.S. Zhu, M. Xue, Q.L. Zhang, J.Y. Sun, X.D. Guo, S.L. Qiu, S.T. Xu, P. Wang, D.J. Wang, Y. Wei, Chem. Eur. J. 12 (2006) 3754.
[44] Q.R. Fang, G.S. Zhu, Z. Jin, M. Xue, X. Wei, D.J. Wang, S.L. Qiu, Angew. Chem. Int. Ed. 45 (2006) 6126.
[45] K. Koh, A.G. Wong-Foy, A.J. Matzger, Angew. Chem. Int. Ed. 47 (2008) 677.
[46] Y.K. Park, S.B. Choi, H. Kim, K. Kim, B.H. Won, K. Choi, J.S. Choi, W.S. Ahn, N. Won, S. Kim, D.H. Jung, S.H. Choi, G.H. Kim, S.S. Cha, Y.H. Jhon, J.K. Yang, J. Kim, Angew. Chem. Int. Ed. 46 (2007) 8230.
[47] G. Ferey, C. Serre, C. Mellot-Draznieks, F. Millange, S. Surble, J. Dutour, I. Margiolaki, Angew. Chem. Int. Ed. 43 (2004) 6296.
[48] X.S. Wang, S.Q. Ma, D.F. Sun, S. Parkin, H.C. Zhou, J. Am. Chem. Soc. 128 (2006) 16474.
[49] Qianrong Fang, PhD thesis, Jilin University, 2007.
[50] D. Bradshaw, J.B. Claridge, E.J. Cussen, T.J. Prior, M.J. Rosseinsky, Acc. Chem. Res. 38 (2005) 273.
[51] B. Kesanli, W.B. Lin, Coord. Chem. Rev. 246 (2003) 305.
[52] D.N. Dybtsev, A.L. Nuzhdin, H. Chun, K.P. Bryliakov, E.P. Talsi, V.P. Fedin, K. Kim, Angew. Chem. Int. Ed. 45 (2006) 916.
[53] K. Biradha, C. Seward, M.J. Zaworotko, Angew. Chem. Int. Ed. 38 (1999) 492.
[54] J.S. Seo, D. Whang, H. Lee, S.I. Jun, J. Oh, Y.J. Jeon, K. Kim, Nature 404 (2000) 982.

[55] C.D. Wu, A. Hu, L. Zhang, W. Lin, J. Am. Chem. Soc. 127 (2005) 8940.
[56] G. Tian, G.S. Zhu, X.Y. Yang, Q.R. Fang, M. Xue, J.Y. Sun, Y. Wei, S.L. Qiu, Chem. Commun. (2005) 1396.
[57] D.L. Long, A.J. Blake, N.R. Champness, C. Wilson, M. Schroder, J. Am. Chem. Soc. 123 (2001) 3401.
[58] W.S. Liu, T.Q. Jiao, Y.Z. Li, Q.Z. Liu, M.Y. Tan, H. Wang, L.F. Wang, J. Am. Chem. Soc. 126 (2004) 2280.
[59] B.Q. Ma, D.S. Zhang, S. Gao, T.Z. Jin, C.H. Yan, G.X. Xu, Angew. Chem. Int. Ed. 39 (2002) 3644.
[60] C. Serre, N. Stock, T. Bein, G. Ferey, Inorg. Chem. 43 (2004) 3159.
[61] G. Mancino, A.J. Ferguson, A. Beeby, N.J. Long, T.S. Jones, J. Am. Chem. Soc. 127 (2005) 524.
[62] X.D. Guo, G.S. Zhu, Q.R. Fang, M. Xue, G. Tian, J.Y. Sun, X.T. Li, S.L. Qiu, Inorg. Chem. 44 (2005) 3850.
[63] X.D. Guo, G.S. Zhu, F.X. Sun, Z.Y. Li, X.J. Zhao, X.T. Li, H.C. Wang, S.L. Qiu, Inorg. Chem. 45 (2006) 2581.
[64] X.D. Guo, G.S. Zhu, Z.Y. Li, Y. Chen, X.T. Li, S.L. Qiu, Inorg. Chem. 45 (2006) 4065.
[65] X.D. Guo, G.S. Zhu, Z.Y. Li, F.X. Sun, Z.H. Yang, S.L. Qiu, Chem. Commun. (2006) 3172.
[66] Ying Wang, PhD thesis, Jilin University, 2009.
[67] X.J. Yin, G.S. Zhu, W.S. Yang, Y.S. Li, G.Q. Zhu, R. Xu, J.Y. Sun, S.L. Qiu, R.R. Xu, Adv. Mater. 17 (2005) 2006.
[68] H.L. Guo, G.S. Zhu, H. Li, X.Q. Zou, X.J. Yin, W.S. Yang, S.L. Qiu, R.R. Xu, Angew. Chem. Int. Ed. 45 (2006) 7053.
[69] H.L. Guo, G.S. Zhu, I.J. Hewitt, S.L. Qiu, J. Am. Chem. Soc. (2009), Revised.
[70] S. Hasegawa, S. Horike, R. Matsuda, S. Furukawa, K. Mochizuki, Y. Kinoshita, S. Kitagawa, J. Am. Chem. Soc. 129 (2007) 2607.
[71] M. Jacoby, Chem. Eng. 86 (2008) 13.
[72] D.J. Collins, H.C. Zhou, J. Mater. Chem. 17 (2007) 3154.
[73] N.L. Rosi, J. Eckert, M. Eddaoudi, D.T. Vodak, J. Kim, M. O'Keeffe, O.M. Yaghi, Science 300 (2003) 1127.
[74] A.G. Wong-Foy, A.J. Matzger, O.M. Yaghi, J. Am. Chem. Soc. 128 (2006) 3494.
[75] E.C. Spencer, J.A.K. Howard, G.J. McIntyre, J.L.C. Rowsell, O.M. Yaghi, Chem. Commun. (2006) 278.
[76] F.M. Mulder, T.J. Dingemans, M. Wagemaker, G.J. Kearley, Chem. Phys. 317 (2005) 113.
[77] S. Bordiga, J.G. Vitillo, G. Ricchiardi, L. Regli, D. Cocina, A. Zecchina, B. Arstad, M. Bjrgen, J. Hafizovic, K.P. Lillerud, J. Phys. Chem. B 109 (2005) 18237.
[78] F.M. Mulder, T.J. Dingemans, H.G. Schimmel, A.J. Ramirez-Cuesta, G.J. Kearley, Chem. Phys. 351 (2008) 72.
[79] J.L.C. Rowsell, O.M. Yaghi, Angew. Chem. Int. Ed. 44 (2005) 4670.
[80] M. Latroche, S. Surble, C. Serre, C. Mellot-Draznieks, P.L. Llewellyn, J.H. Lee, J.S. Chang, S.H. Jhung, G. Ferey, Angew. Chem. Int. Ed. 45 (2006) 8227.
[81] J.L.C. Rowsell, O.M. Yaghi, J. Am. Chem. Soc. 128 (2006) 1304.
[82] S.Q. Ma, D.F. Sun, M. Ambrogio, J.A. Fillinger, S. Parkin, H.C. Zhou, J. Am. Chem. Soc. 129 (2007) 1858.
[83] M. Xue, S.Q. Ma, Z. Jin, R.M. Schaffino, G.S. Zhu, E.B. Lobkovsky, S.L. Qiu, B.L. Chen, Inorg. Chem. 47 (2008) 6825.
[84] M. Dinca, J.R. Long, Angew. Chem. Int. Ed. 47 (2008) 6766.
[85] M. Dinca, J.R. Long, J. Am. Chem. Soc. 129 (2007) 11172.
[86] M. Dinca, W.S. Han, Y. Liu, A. Dailly, C.M. Brown, J.R. Long, Angew. Chem. Int. Ed. 46 (2007) 1419.
[87] M. Xue, G.S. Zhu, Y.X. Li, X.J. Zhao, Z. Jin, E. Kang, S.L. Qiu, Cryst. Growth Des. 8 (2008) 2478.
[88] M. Kondo, T. Okubo, A. Asami, S. Noro, T. Yoshitomi, S. Kitagawa, T. Ishii, H. Matsuzaka, K. Seki, Angew. Chem. Int. Ed. 38 (1999) 140.
[89] S. Noro, S. Kitagawa, M. Kondo, K. Seki, Angew. Chem. Int. Ed. 39 (2000) 2082.
[90] S.Q. Ma, D.F. Sun, J.M. Simmons, C.D. Collier, D.Q. Yuan, H.C. Zhou, J. Am. Chem. Soc. 130 (2008) 1012.
[91] L. Pan, B. Parker, X.Y. Huang, D.H. Olson, J. Lee, J. Li, J. Am. Chem. Soc. 128 (2006) 4180.
[92] L. Pan, D.H. Olson, L.R. Ciemnolonski, R. Heddy, J. Li, Angew. Chem. Int. Ed. 45 (2006) 616.
[93] B.L. Chen, C.D. Liang, J. Yang, D.S. Contreras, Y.L. Clancy, E.B. Lobkovsky, O.M. Yaghi, S. Dai, Angew. Chem. Int. Ed. 45 (2006) 1390.
[94] S.Q. Ma, D.F. Sun, X.S. Wang, H.C. Zhou, Angew. Chem. Int. Ed. 46 (2007) 2458.
[95] R. Matsuda, R. Kitaura, S. Kitagawa, Y. Kubota, R.V. Belosludov, T.C. Kobayashi, H. Sakamoto, T. Chiba, M. Takata, Y. Kawazoe, Y. Mita, Nature 436 (2005) 238.
[96] A.J. Fletcher, E.J. Cussen, D. Bradshaw, M.J. Rosseinsky, K.M. Thomas, J. Am. Chem. Soc. 126 (2004) 9750.
[97] R. Vaidhyanathan, D. Bradshaw, J.N. Rebilly, J.P. Barrio, J.A. Gould, N.G. Berry, M.J. Rosseinsky, Angew. Chem. Int. Ed. 45 (2006) 6495.
[98] F. Schroeder, D. Esken, M. Cokoja, M.W.E. van den Berg, O.I. Lebedev, G. van Tendeloo, B. Walaszek, G. Buntkowsky, H.H. Limbach, B. Chaudret, R.A. Fischer, J. Am. Chem. Soc. 130 (2008) 6119.
[99] Y.K. Hwang, D.Y. Hong, J.S. Chang, S.H. Jhung, Y.K. Seo, J. Kim, A. Vimont, M. Daturi, C. Serre, G. Férey, Angew. Chem. Int. Ed. 47 (2008) 4144.
[100] S. Horike, M. Dinca, K. Tamaki, J.R. Long, J. Am. Chem. Soc. 130 (2008) 5854.
[101] M.H. Alkordi, Y.L. Liu, R.W. Larsen, J.F. Eubank, M. Eddaoudi, J. Am. Chem. Soc. 130 (2008) 12639.
[102] D. Maspoch, D. Ruiz-Molina, K. Wurst, N. Domingo, M. Cavallini, F. Biscarini, J. Tejada, C. Rovira, J. Veciana, Nat. Mater. 2 (2003) 190.
[103] S.S. Kaye, H.J. Choi, J.R. Long, J. Am. Chem. Soc. 130 (2008) 806.
[104] T.M. Reineke, M. Eddaoudi, M. O'Keeffe, O.M. Yaghi, Angew. Chem. Int. Ed. 38 (1999) 2590.
[105] B.L. Chen, Y. Yang, F. Zapata, G.N. Lin, G.D. Qian, E.B. Lobkovsky, Adv. Mater. 19 (2007) 1693.
[106] F. Marlow, M.D. McGehee, D.Y. Zhao, B.F. Chmelka, G.D. Stucky, Adv. Mater. 11 (1999) 632.